Computation of High Reynolds Number Flows Using Vorticity Confinement: I. Formulation

John Steinhoff[1], Nicholas Lynn[2] and Lesong Wang[3]

Abstract

A computational method is described that has been designed to capture thin vortical regions in high Reynolds number incompressible flows. The principal objective of the method—Vorticity Confinement (VC)—is to capture the *essential* features of these small-scale vortical structures and model them with a very efficient difference method *directly* on an Eulerian computational grid. Essentially, the small scales are modeled as *nonlinear solitary waves* that "live" on the lattice indefinitely. The method allows convecting structures to be modeled over as few as 2 grid cells with no numerical spreading as they convect indefinitely over long distances, with no special logic required for merging or reconnection.   It also serves as a very efficient substitute for RANS models of attached and separating boundary layers and vortex sheets and filaments. Further, the method easily allows boundaries with no-slip conditions to be treated as "immersed" surfaces in uniform, non-conforming grids, with no requirements for complex logic involving "cut" cells.

In this paper a description of the basic VC method is given. This is more comprehensive than has been previously available. There are close analogies between VC and well-known shock and contact discontinuity capturing methodologies. These are discussed to explain the basic ideas behind VC, since it is somewhat different than conventional CFD methods. Some of the possibilities that VC offers towards very efficient computation of turbulent flows in the LES approximations are explored. These stem from the ability of VC to act as a negative dissipation at scales just above a grid cell, but that saturates and does not lead to divergence. This feature allows

1. approximate cancellation of numerical diffusion, so that more complex, high order-low dissipation schemes can be avoided. Small-scale vortical structures at the grid cell level can then be captured, resulting in very efficient use of the available degrees of freedom on the grid.
2. approximate treatment of backscatter. This involves the addition of (modeled) subgrid kinetic energy to the flow in a natural way, without requiring stochastic forcing, and which restores some of the instabilities that are removed by the (implicit) filtering.

Although used for a number of years for complex, attached and separating flows, and trailing vortices, its use as an LES method is relatively recent. In Ref. [0], some initial LES results are presented.

1 Introduction

We describe the Vorticity Confinement (VC) method for efficiently treating thin vortical structures in high Reynolds number incompressible flow. This forms the basis of the VC-based LES, or "VCLES" method for turbulent flow simulation, which is the subject of this paper. Earlier applications of VC have included capturing attached and separating boundary layers and convecting vortex sheets and filaments. These have served as a substitute for much more expensive RANS schemes, and are described in the literature [15]. This study involves turbulent flow simulations, where VC is used in the modeling and computation of the thin vortex filaments and sheets, which we assume to be the smallest resolved scales.

The principal objective of VC is to capture the *essential* features of these small-scale vortical structures. By essential features, we mean vortex filaments that may convect over long distances with no significant spreading and can change topology and merge or reconnect and can absorb large-scale energy by stretching; and vortex sheets that can become unstable and break up into filaments. As such, it can be thought of as "physical structure preserving". This is affected with a very efficient difference method *directly* on a (fixed Eulerian) computational grid. It is argued that this is more effective than first formulating a model partial differential equation (pde) for these small scales and then making a discrete approximation, since it allows thin vortical regions to be implicitly modeled, spread over as

---

[1] Professor, The University of Tennessee Space Institute, Tullahoma, TN
[2] Graduate Research Assistant, The University of Tennessee Space Institute, Tullahoma, TN
[3] Research Scientist, Flow Analysis, Inc.

few as 1-3 grid cells, and convected over arbitrarily long distances with no effects due to numerical error. The irrotational part of the flow, as well as any larger scale vortical structures, can then be solved with sufficient resolution with conventional, discretized partial differential equations (Euler equations). For these regions, the method can reduce to conventional computational fluid dynamics (CFD).

Besides allowing simple coarse grids to be used, the method can be used effectively with low order time and space discretization of the basic equations, since it eliminates artificial spreading due to numerical diffusion for the small vortical scales. This greatly simplifies boundary conditions and reduces computational time further.

The purposes of this paper are to explain the basic rationale behind using VC, to describe the main ideas behind VC in more detail than has been available in previous papers, and finally, to explore the possibilities that it offers towards more efficient LES computations of turbulent flows. Some initial LES results are presented in Ref. [0].

1.1 Basic Rationale

First, our basic overall objectives for turbulent flow simulations will be described. The goal of any LES method is, of course, to solve for the larger scales of turbulent flow and obtain a solution of a filtered, or convolved flow field with the small scales filtered out. There are two basic concepts in an LES method that we assume to be important and which serve as the rationale for using VC:

First, for small scale vortices, VC allows us to reduce numerical dissipation so that it minimizes the effect on the numerical solution, down to scales of a small number (~2) of grid cells sizes (h), so that other nearby scales - as small as ~3-4h, are not significantly contaminated. In this way, VC allows us to maximize h for a given resolution, or effective filter width. This is important because every factor of 2 increase in h leads to a factor of 16 decrease in computing time. For general small vortical scales, it is not possible to avoid numerical error over long convection times, even if expensive high order conventional CFD schemes are used. However, if the small scales in the field consist of vortex sheets and filaments, as is often assumed, this is easily accomplished – with VC.

Second, even in the limit of vanishing viscosity, just eliminating numerical errors, such as diffusion, and accurately solving the Euler equations for the filtered field is not sufficient. A filtered field computed in this way would not experience as strong instabilities as the unfiltered field would. This reduction of instabilities can have strong consequences, even in 2-D flows. Thus, these instabilities must be restored by a destabilizing term, which can be accomplished with VC. The basic idea will be (qualitatively) discussed below for Kelvin-Helmholtz (KH) flows, as an example. This issue essentially involves approximating backscatter.

Kelvin Helmholtz Instability

Consider a flat 2-D contact discontinuity (vortex sheet) along the x axis, with velocity u = +1 above and –1 below, and v=0. The kinetic energy density

$$e = \vec{q}^2 / 2 = u^2 / 2 = 1/2$$

both above and below the sheet. Now consider a filtered field (Fig. 1); e will have the form in Fig. 2 with the dashed curve representing the unfiltered field and the solid, the filtered field. The area between the solid and dashed curves represents sub-grid scale, or "latent" energy that is not present in the filtered field. This energy should be considered since it can be added to the filtered field as it evolves to energize the KH instabilities that have been damped by the filtering.

The unfiltered sheet will, of course, be unstable to an imposed perturbation, which will initially grow exponentially and then tend to saturate (by the sheet rolling up). The physical realization of this is the set of small, rolling up vortex sheets sketched in Fig. 3. The LES goal is, of course, to evolve the filtered velocity field to represent this phenomenon. Thus, an initially thick vortex layer (representing the filtered initial sheet) should be unstable and evolve to a set of vorticity concentrations, which represent the filtered spirals. These should also initially grow exponentially and then saturate, as sketched by the vorticity contours in Fig. 4. Computations of a similar case are described in Section 3.1.3.

However, even if the filtered field evolves exactly according to the Euler equations, with no numerical error, it will have to evolve over a longer time period than the unfiltered field before exhibiting such vorticity instabilities. Also in 2-D inviscid, incompressible flow (obeying Euler equations alone), it is well known that vorticity is only convected without changing magnitude. Thus regions of increased magnitude cannot develop. We conclude that the filtered field should evolve according to the Euler equations, but with a negative dissipation added that will also cause it to be unstable initially, but that will eventually saturate and not diverge. This extra term should involve an acceleration of the flow or energizing of the developing vorticity concentrations, leading eventually to a set of separated vortices. The total energy will then have increased over that of the initial thick, flat sheet. A possible approximation, or basis for this model would be that the final energy gain of the filtered field, which is determined

by the initial field and the final vortices, should represent the subgrid, or "latent" energy present initially. Currently, we only use this idea as a qualitative guide, but are beginning to develop more quantitative methods.

The main point is that the VC represents a very simple way to add the required energy and, at the same time, eliminate the spreading effects of numerical dissipation.

2. Vorticity Confinement – Basic Concepts

The basic VC concept is related to that of similar methods also involving thin structures – shock and contact discontinuity capturing. Accordingly, before describing the VC method, analogous, relevant features of these methods will be briefly described, since they have been used extensively for some time and are very familiar to the CFD community. Then, basic concepts of the new method (VC) will be reviewed. These points are known to people familiar with VC and more conventional discontinuity capturing methods, but may be helpful to people to whom it is new. We will use shock capturing as an example.

Shock capturing methods have, of course, received an extremely large amount of attention in the CFD community and have proven to be extremely important. These methods typically use only a moderately sized inviscid computational grid in the shock region. This is possible because only the *essential* physics of the shock (as far as the flow problem being solved) is retained. By "essential physics" we mean those features that affect the flow external to the shock interior. These features include computed shock thickness, which does not have to be as small as the physical thickness but, like the physical thickness, must be small compared to the main length scales of the problem. They also include the requirement that conservation laws, integrated through the shock, are preserved. In this way, for many problems that do not depend on the details of the shock internal structure, accurate flow solutions have been obtained with specially developed numerical "shock capturing" algorithms. In these methods the detailed, accurate solution of partial differential equations (pde)'s (for example, Navier-Stokes equations) for the internal shock structure have been avoided. This has been important since it avoids the requirements of a very fine computational grid within the structure, and very time consuming viscous computations there. These ideas, which go back to Von Neumann and Richtmyer [1], Lax [2] and others, involve the concept of "weak solutions" of pde's where, in the inviscid limit, discontinuous features can be treated. After discretization these ideas should allow shocks to be approximated over as few as 1-3 grid cells.

The question naturally arises as to whether similar efficient "capturing" treatments of thin vortical features are also possible, which would result in similar benefits. One difference, however, is that with shocks, unlike vortical regions, characteristics slope inward toward the shock, which naturally tends to steepen during a computation. As a result, modeling shocks is simpler than modeling thin vortical structures and other contact-like discontinuities which naturally tend to spread due to numerical discretization errors and the need for stabilizing numerical diffusion. This results in the requirement that a "steepening" or "Confinement" term be added to prevent artificial spreading.

The method described in this paper—VC—has been specifically formulated to effectively treat the difficult-to-compute concentrated vortical regions with the same basic philosophy as shock capturing. Although developed independently, the method, in its one–dimensional form, has some relation to Harten's "artificial compression" scheme for one-dimensional compressible flow [3]. However, the VC formulation is much simpler (at least for incompressible flows). Also, an important feature for capturing thin vortical regions is that VC is intrinsically multidimensional and rotationally invariant [3,4]. A number of recent papers [5-12], mentioned below, describe the use of VC for incompressible flow. Further extensions to compressible flow have been recently developed [13-16] but will not be described here, since we want to concentrate on turbulent flow with as few extra complications as possible. As with shock capturing, it is understood that the details of the internal structure of thin vortical regions will not be accurately treated, unless special models are developed for them. We assume here that these details are not important, other than possibly subgrid scale energy of thin sheets, and that simple capturing alone is sufficient.

As background, we first mention some previous (non-LES) examples for which VC alone is effective. These include convecting vortex rings, which can be convected with no spreading, yet can merge with no requirement for special logic [7]. They also include thin shed wingtip vortices which can be computed over arbitrarily long distances [17, 39] and exhibit Crow instability, including merging [17]. Computations of both of the above phenomena show close agreement with experiment. For trailing vortex convection over very long distances (many kilometers) the method can serve as a zeroth order approach in this case, since turbulence eventually induces a very slow spreading. This effect can then be simply modeled within the VC framework, again without using very fine grids or high order methods. Examples also include a very simple and inexpensive RANS substitute for attached and separating boundary layers. This is described below in Sec. 3.1.4 and in Refs. [15,18-20].

An important point that should be emphasized is that, at high Re most vortical regions will be turbulent. Hence, *any* computational method must involve, explicitly or implicitly, a numerical model for the small-scale structure,

since it is not feasible to directly solve the Navier-Stokes equations for this structure. The structure obtained with VC when a small-scale vortical region or "eddy", is captured can, thus, be thought of as just such a model, but one that is very efficient to compute. Further, this model is intrinsically discrete, defined over only a few grid cells, and is not meant to be an accurate solution of a model pde. The rationale for taking this approach is that it is difficult to resolve pde's for a thin vortical structure over long distances, even with higher order methods, if it is spread over only a small number of grid cells (2-4). This is due to the well-known fact that the accuracy, or *order*, of a method is only an *asymptotic* estimate of the behavior of the error, valid for large N, the number of grid cells across the vortical region. N=2-3 is not sufficient to apply such an estimate. Since VC is meant to *capture* the feature, and not accurately solve a model pde, it gets around this problem. Further, many features of the flow external to the core, or interior of a vortical region are not sensitive to the details of the internal structure. For example, in 2-D, vortices tend to evolve to an axially symmetric state [32]. Then, the only requirements for accurately determining the induced flow external to the initial core are that the total circulation is conserved, that the vortex centroid have the correct location, and that the core does not spread due to numerical effects.

As stated VC even involves a negative, though non-diverging, *total* diffusion at certain length scales. Similar observations about the need for such a negative total dissipation, or eddy viscosity in LES for certain regions of the flow have been made in Refs. [36]. These authors explain that in those regions, popular models for the eddy viscosity cannot be used because conventional numerical methods for solving the flow equations would diverge there. As a result, the eddy viscosity is often arbitrarily set to zero in those regions. One of the main advantages of VC is that it allows an overall negative eddy viscosity to be implemented - which ultimately saturates, rather than diverges.This approach should be much simpler and more direct than other approaches used to treat negative diffusion, or, effectively, energize the small scale vortices, such as "stochastic forcing".

There are currently other efforts to capture small scales directly on the grid for use in LES turbulence simulations. These often involve combinations of one-dimensional operators, as in original discontinuity capturing schemes [3-4, 25] – they are known, appropriately, as "Implicit Large Eddy Simulation", or ILES [26]. As opposed to VC, the emphasis in these is typically not on vorticity. Also, their main goal is to cancel numerical diffusion as much as possible [26], whereas for VC it is to specifically treat thin vortical structures with a controlled "model" structure.

2.1 Illustrative One-Dimensional Example

As explained in the last section, the basic concept of VC is that thin vortices are "captured", like shocks, over only a few grid cells. This means, of course, that the discrete equations do not represent an accurate solution of a simple pde for the internal structure, although they can be considered as approximations to singular (weak) solutions. The goal in these cases (for small scales) is to only accurately treat certain integral quantities, and to be "physical structure preserving" (i.e., ensure that the vortex remains thin).

There is a simple example of this concept in one dimension involving the convection of a passive scalar, or "pulse" that is concentrated in a small region. A goal, then, could be to preserve the total amplitude of this scalar, to have the centroid move at the correct convection speed, and to ensure that it remains compact—essentially spread over a small number of cells. Additional moments of this pulse representing additional structure could, if desired, also be transported using additional fields, but no attempt is made at convecting an accurate, point-wise representation of the internal structure.

It will be seen that the solution of the "confined" equations is, effectively, a nonlinear *solitary wave* that "lives" on the lattice indefinitely. The same applies to the VC solutions of convecting vortices, although, of course, they cannot be analyzed in as much detail as this 1-D example.

We then consider a scalar (ϕ) advecting at a speed c that, in the continuum case, would satisfy the pde

$$\partial_t \phi = -\partial_x c\phi \ . \qquad (2.1)$$

Symbolically, we then define a discretized equation:

$$\phi_j^{n+1} = \phi_j^n - \Delta t C \phi_j^n + E_j^n \ , \qquad (2.2)$$

where C is a conventional conservative discrete convection operator, j denotes spatial grid index, n the timestep ($t = n\Delta t$), and E_j^n is a non-linear term designed to keep the pulse compact.

There are requirements for E_j^n if the total pulse amplitude and speed are to be conserved, independent of the pulse amplitude:

1. E_j^n must be (at least) a first difference to conserve the total amplitude (which is assumed to vanish rapidly away from the centroid).

2. E_j^n must be (at least) a second derivative so that, each timestep, the centroid position is not changed by E_j^n and, hence, the speed of the centroid is correct, as given by the original pde. Then,

$$E_j^n = \delta_j^2 F_j^n \qquad (2.3)$$

3. where δ_j^2 is a discrete second difference operator and F_j^n is a function of ϕ and its differences, which vanishes in the far field.

4. F_j^n must be homogeneous of degree 1 in ϕ, as the other terms in the equation, so that there is no dependence on the amplitude, or scale of ϕ.

5. $\delta_j^2 F_j^n$ must represent a negative diffusion if the pulse is spread over too large an area, so that it contracts and relaxes to a fixed shape.

6. $\delta_j^2 F_j^n$ must become a positive diffusion if the pulse is too thin, for the same reasons.

Property (4) requires that F_j^n be non-linear. If it were linear, the negative diffusion would result in divergence: Any modes that initially increase in amplitude would continue to increase and eventually diverge since they would be uncoupled and would evolve independently.

A simple formulation that satisfies the above requirements is:

$$C\phi_j^n = \frac{\delta_j^c c_j \phi_j^n}{h} \quad (2.4)$$

$$F_j^n = \mu \phi_j^n - \varepsilon \Phi_j^n \qquad (2.5)$$

where δ_j^c is a central difference, h is the grid cell size, μ and ε are constants, and Φ_j^n is a harmonic mean:

$$\Phi_j^n = \left[\frac{\sum_{j-1}^{j+1} \left(\phi_l^n \right)^{-1}}{3} \right]^{-1} . \qquad (2.6)$$

There are many other formulations for F that also can be used. The first term in F_j^n acts to stabilize the central difference operator C and also satisfies conditions (1-3) and (5), and the second term satisfies conditions (1-4) and (6).

The resulting difference equation can be written

$$\phi_j^{n+1} = \phi_j^n - \frac{1}{2} \left(v_{j+1} \phi_{j+1}^n - v_{j-1} \phi_{j-1}^n \right) + \delta_j^2 \left(\mu \phi_j^n - \varepsilon \Phi_j^n \right) \qquad (2.7)$$

where δ_j^2 is a second difference operator and

$$v_j = c_j \Delta t / h . \qquad (2.8)$$

Results of a computation (on a periodic – 256 cell grid) with no Confinement, using $\mu = .2$ and $\varepsilon = 0$. after 100 time steps (1/10th pass through the grid) are shown in Fig. 5. (Of course, higher order conventional CFD methods could result in less diffusion than shown here. However, compared to Confinement, these would all require more grid cells within the pulse and, eventually, spread it over even more cells due to accumulated numerical error.) Results are also shown in Figure 5 with Confinement for 1 and 100 passes through the grid for $\mu = .2$ and $\varepsilon = .5$. For all of these cases, $v = \sqrt{2}/6$, chosen to be irrational to prevent coincidental error cancellation.

The exact "sampled" pulse height at any given time step depends on the centroid position within a grid cell, almost as if an approximately fixed pulse shape were "moved" through the grid and the values sampled at each time step. The pulse, however, remains confined indefinitely, except for a very small effect (after $\sim 10^6$ time steps) due to the finite precision of the computer. This implies that there is an approximate, smooth solution to Equation 2.7, $\phi(x,t)$, in terms of a similarity variable, $z = x - ct$. For a range of initial conditions that have the form of a thin pulse, ϕ will relax to this particular "solitary wave" pulse solution. This has been shown numerically. However, stability of the solitary wave and the set of initial conditions that are attracted to it have not been mathematically derived.

It has been shown [21] that, for a range of values of μ, ε and ν, the sign of ϕ cannot change. Thus for an initial non-negative pulse, the maximum cannot exceed the sum, which is conserved. This prevents the solution from diverging.

In the small Δt limit, for constant c, ϕ satisfies

$$\delta_j^2 \left(\mu \phi_j^n - \varepsilon \Phi_j^n \right) = 0 . \qquad (2.9)$$

A solution is then

$$\phi_j^n = A \operatorname{sech} \left(\gamma \left(x - x_0 - ct \right) \right) \quad (2.10)$$

where A and x_0 depend on initial amplitude and centroid, and

$$\cosh \left(\gamma \right) = \left(\frac{3\varepsilon}{\mu} - 1 \right) \Big/ 2 . \qquad (2.11)$$

It will be shown in Sec. 3.2 that Equations 2.6 and 2.7, when summed over $j' < j$, represent a propagating step function—like discontinuity, rather than a pulse. The summed form then exhibits some similarity to schemes used by Harten [3], Van Leer [4] and others to capture one dimensional contact discontinuities and shocks in compressible flow.

3 Vorticity Confinement Methodology

Two formulations of VC have been developed which have similar properties: The first, "VC1", involves first derivatives of velocity [5, 30], while the second, "VC2" involves second derivatives [21]. Starting from an initial condition more spread than the final structure, VC1 acts essentially as an inward convection and relaxes to the final structure more quickly than VC2, which acts, initially as a negative, second order diffusion. The two versions will be described below.

The basic principle in VC, as in the one-dimensional convecting scalar example described above, is that there is a solution with a stable structure that can be propagated indefinitely. Although the VC equations can be written as a discretization of a pde (described below), the resulting *solution* at the small scales (within the structure) is not meant to be an accurate, or even approximate solution of the original pde. This is because VC is meant to capture, or model the small scale features over only a couple of grid cells, so that the discretization "error" is O(1) there. As explained in Sec. 1, the features essential for the problem, however, are still preserved. As such, the captured feature is actually a non-linear *solitary wave* that "lives" on the grid lattice. (There is currently a large amount of work being done on intrinsically discrete—or *difference*, as opposed to *finite difference,* equations, examples can be found in Ref [31]). In smooth regions (or for large scales), on the other hand, VC can be made to automatically revert to conventional CFD where the pde's are then accurately and efficiently approximated.

For thin vortical regions in incompressible flow, we use essentially the same approach as in the one-dimensional example above: "Confinement" terms are added to the conventional, discretized momentum equation. Although we use a primitive variable, and not a vorticity, formulation, we will see that if we look at the resulting vorticity transport equation (for the VC2 version, to be described below), it has the identical "Confinement" terms as a multidimensional extension of the one-dimensional scalar transport equation described in Section 2. For general unsteady incompressible flows, the governing equations with Vorticity Confinement are discretisations of the continuity and momentum equations, with added terms:

$$\nabla \cdot \vec{q} = 0 \qquad (3.1)$$

$$\partial_t \vec{q} = -\vec{\nabla} \cdot (\vec{q}\vec{q}) + [\mu \nabla^2 \vec{q} - \varepsilon \vec{s}] \qquad (3.2)$$

where $\vec{q}$ is the velocity vector, p is the pressure, ρ is the density, and μ is a diffusion coefficient that includes numerical effects due, for example, to discretization of the first right hand side (convection) term. (We assume that the Reynolds number is large and that physical diffusion is much smaller than the added terms). For the last term, $\varepsilon \vec{s}$, ε is a numerical coefficient that, together with μ, controls the size and time scales of the convecting vortical regions or vortical boundary layers and $\vec{s}$ is defined below. For this reason, we refer to the two terms in the brackets as the "confinement terms". The vector $\vec{s}$ is different for the two VC formulations, and is defined below.

Equation 3.2 involves constant μ and ε, which is sufficient for many problems. If these are not constant, such as, for example, when the grid spacing is not constant or models are used for them, then these quantities can be taken inside the differential operators in the corresponding terms, to maintain explicit momentum conservation (in the VC2 formulation).

As in the one-dimensional example the *pair* of confinement terms, which represent spreading, or positive diffusion and "contraction", or negative diffusion, together create the confined structures. Stable solutions result when the two

terms are approximately balanced. In this way, corrections are made each time step to compensate for any perturbations to the vortical structure caused by convection in a non-constant external velocity, discretization error in the convection operator, or the pressure correction. The parameters μ and ε then essentially determine the thickness of the resulting vortical structure and the relaxation rate to that state. It should be emphasized that stable, equilibrium structures result for a wide range of values of these parameters.

In general, for boundary layers and isolated, convecting vortex filaments, computed flow fields *external* to the vortical regions are not sensitive to the internal structures, and hence to the parameters ε and μ, over a wide range of values. For example, a general thin, concentrated vortex will physically tend to evolve to an axisymmetric configuration [32]. Further, even a rapidly rotating non-symmetric configuration will be approximately axisymmetric when averaged over a short time [33]. Then, it is well known that the flow outside an axisymmetric two-dimensional vortex core is independent of the vortical distribution, and hence will not depend on ε and μ as long as the core is thin (and the filament curvature is large, so that the flow is approximately two-dimensional in a plane normal to the filament). Therefore, the issues involved in setting these parameters will be similar to those involved in setting numerical parameters in other standard computational fluid dynamics schemes, such as artificial dissipation in many conventional shock-capturing schemes, which, as explained, are closely analogous. Further, for turbulent wake flows, preliminary studies - described in Ch. 12, suggest that ε can be used to parameterize finite Reynolds number effects, since it controls the intensity of the smallest resolved vortical scales (this is the subject of current research [22]). This parameter can also be used to adjust the confinement level according to the amount of available sub-grid energy (this is also a subject of current research).

An important feature of the Vorticity Confinement method is that, for incompressible flow, the Confinement terms are non-zero only in the vortical regions, since both the diffusion term and the "contraction" term vanish outside those regions. Thus, even if there is a second order isotropic numerical diffusion associated with the convection operator, and the diffusion operators are only second order, outside the vortical regions the resulting accuracy of these terms can be third or fourth order, since this diffusion is just the negative curl of the vorticity.

A final point concerns the total change induced by the VC correction in mass, vorticity and momentum, integrated over a cross section of a convecting vortex. A pressure – projection method [34] is used to solve eqns. 3.1 and 3.2, so that mass is automatically conserved. Vorticity is explicitly conserved because of the vanishing of the correction outside the vortical regions. Finally, (in the VC2 formulation), momentum is also exactly conserved [21] because the VC terms added to the momentum equations have a spatial derivative operator in front. In the 1-D example described above, this ensures that the pulse centroid convects with a weighted average of the imposed velocity. This should also be true for a confined vortex convecting in an imposed external velocity field. Then, the vortex centroid will move with a weighted average of the velocity of the "background" flow, with no effect due to self-induced flow (at least in 2-D). This has been demonstrated numerically [20, 35] (see Section 3.1.2). This is not exactly satisfied in the VC1 formulation, but errors due to the lack of momentum conservation have been shown numerically to be small in most cases (see Sec. 3.1.1).

Many basic numerical methods could be used for space and time discretization. We use a simple first order Euler integration in time and second order in space with, as stated, a pressure – projection method to enforce mass conservation. In conventional CFD schemes higher order methods often must be used, usually to reduce numerical diffusion and hence attempt to reduce spreading of thin vortical regions. Vorticity Confinement eliminates this problem for many cases and avoids the boundary condition complexity and computational cost of the higher order methods. (It should be mentioned, however, that the second confinement, or contraction term involves a larger difference stencil than the other terms).

Another numerical issue involves the regularity of the grid. It is important to realize that, since a convecting vortex or separated boundary layer is captured directly on the grid, over a few grid cells, large grid aspect ratios or rapidly varying cell sizes should not be used. If these are avoided, VC will result in a dynamics that is close to rotationally invariant. These issues also occur, of course, in shock capturing. Some modifications can be made, however, to accommodate non-uniform grids if the aspect ratio is not too large (38, 45, 46).

3.1 Basic Formulation

As explained, the two different formulations, VC1 and VC2, have somewhat different dynamics, since they differ in the order of the derivative in the contraction term. The one developed initially (VC1) has been described in a number of publications and only a few details will be presented here.

3.1.1 VC1 Formulation

This formulation involves an expression for the "contraction term", $\vec{s}$, that does not explicitly conserve momentum:

$$\vec{s} = \hat{n} \times \vec{\omega} . \tag{3.3}$$

For convecting vortices,

$$\hat{n} = \vec{\nabla}\eta \Big/ \left| \vec{\nabla}\eta \right| \tag{3.4}$$

where

$$\eta = \left| \vec{\omega} \right| .$$

For boundary layers, $\hat{n}$ is a unit vector parallel to the local normal. This term essentially convects vorticity within a thin vortical region either along its own gradient or along the local normal, from the edge, or region of lower magnitude, toward the center, or region of larger magnitude. As the structure contracts and the gradient increases, the "expansion" term, which is a linear diffusion, increases until a balance is reached. (This is a well-known property of convection-diffusion phenomena.) Due to the rapid rotation of convecting concentrated vortices, any non-conservative momentum errors are almost completely canceled and the method has proved to be sufficiently accurate for many problems.

A technicality in applying this method is often overlooked by people using it: this was described in earlier papers [30]. Since vorticity is convected along $\hat{n}$, upwind (in $\hat{n}$) values of ω should be used in the contraction term to avoid creating "downwind" values of vorticity with an opposite sign. This is easily accomplished with weighting factors at each node that depend on $\hat{n}$ and unit vectors to neighboring grid nodes.

Most of the VC results presented in the literature use the VC1 formulation. However, they do not involve very slow background flow and do not involve the momentum conservation issue discussed below. An important point, however, is that exact momentum conservation, in some cases, may not be as important as other features (such as, in our case, ensuring that a convecting vortex remain thin) and should not be regarded as an absolute requirement (see, for example, the basic CFD textbook - Tannehill, Anderson and Pletcher [28], pg. 60).

3.1.2 VC2 Formulation

Only for very accurate long-term trajectory determination of vortices convecting in a slow background velocity field has the momentum-conserving VC2 formulation been found to be necessary (for incompressible flow). This ensures that the contribution of the self-induced velocity to the vortex motion is completely canceled.

The VC2 formulation involves

$$\vec{s} = \vec{\nabla} \times \vec{w}^n . \tag{3.5}$$

We can also combine the dissipation and the confinement into a single term:

$$\mu \nabla^2 \vec{q} - \varepsilon \vec{s} = \nabla \times \left(\mu \vec{\omega}^n - \varepsilon \vec{w}^n \right) \tag{3.6}$$

where

$$\vec{\omega}^n = \vec{\nabla} \times \vec{q}^n \tag{3.7}$$

and

$$\vec{w}^n = \frac{\vec{\omega}^n}{\tilde{\omega}^n} \left[\frac{\sum_l \left(\tilde{\omega}_l^n \right)^{-1}}{N} \right]^{-1} \tag{3.8}$$

$$\tilde{\omega}_l^n = | \bar{\omega}_l^n | + \delta . \tag{3.9}$$

Equation 3.6 has some numerical advantages over the form just above it, since the same difference operator acts on $\vec{\omega}$ and $\vec{w}$. Also, the second confinement term (3.8) is the sum over the stencil which consists of the central node (where $\vec{w}$ is computed) and its neighboring ($N-1$) nodes, and δ is a small positive constant ($\sim 10^{-8}$) to prevent problems due to finite precision.

When two approximately oppositely directed vortices are close to each other, there can be grid cells in between in which $\vec{w}$ is not well defined, which may cause oscillations. To prevent this, if the scalar product of any of the other vorticity vectors in the stencil with the central node is negative, $\vec{w}$ is set to zero.

To see the action of VC2, we take the curl of Equation 3.6. We then get a transport equation for vorticity. For example, in two dimensions,

$$\partial_t \omega = -\nabla \cdot (\omega \vec{q}) + \nabla^2 [\mu \omega - \varepsilon \Phi(\omega)] \qquad (3.10)$$

This equation, including the confinement term, is exactly a multi-dimensional, rotationally invariant generalization of the one-dimensional scalar advection equation shown to be effective in Section 2. Of course, the solution will still reflect the four-fold symmetry of the grid. This effect, however, vanishes rapidly away from a vortical region. Further, the rotating flow around a vortex core actually allows a simpler discretisation of Eqn.3.10, compared to an axisymmetric convecting passive scalar distribution. This is explained in Ref. [21].

Equation 3.8 is a harmonic mean. It is chosen to weigh the small values in the stencil more heavily. As is well known, this term vanishes when any of the values of its argument vanishes, preventing creation of values of opposite sign (for a range of parameters). Using VC, the total vorticity in a region surrounding a vortex is conserved, since it is a local term. This means that the vorticity cannot diverge due to this term, since the maximum absolute value cannot be greater than the absolute value of sum when all values have the same sign. (This is also a property of the one-dimensional scalar advection example.)

There are a large number of alternative forms that would work as well as the harmonic mean. We believe that the term should have a smooth algebraic form, however, to give smooth results. This should be more appropriate for multidimensional applications than forms involving logic functions, such as *"minmod",* which give good results in one-dimensional applications. As discussed above, a harmonic mean term was used by Van Leer [4] as a limiter, but mostly in one-dimensional compressible flow, and, to the author's knowledge, not as a function of vorticity. (The VC1 and VC2 methods were developed independently, as multidimensional, rotationally invariant "Confinement" techniques specifically for thin vortical regions).

3.1.3 Examples of VC Results for Convecting Vortices

Computations were done on a 128x128 uniform Cartesian grid for two vortices of the same strength rotating around each other in 2-D. Results of vorticity contours are presented in Fig. 6 for a sequence of "snapshots" [12]. In Fig. 6a, no confinement was used. The large dissipation of the low order convection numerical method is apparent: In Figs. 6b and 6c, VC2 was used. The thin white lines across the cores represent grid lines. The ability of VC2 to maintain very compact vortices, even after 20 full orbits around each other, is apparent. VC1 shows essentially the same behavior but exhibits some "drifting" over long periods, as expected. It should be emphasized that these results were obtained without resorting to high order methods (which would have been futile on the coarse grid).

As another example, computations were done on a 48x48x48 uniform Cartesian grid for two interacting, initially coplanar vortex rings in 3-D, using VC1 [7]. A vorticity isosurface is shown in Fig. 7, for a sequence of times. The cores can be seen to be confined to about 2 grid cells. In this case, the vortices merge and re-link, with no requirement for special logic. The vorticity isosurfaces from an experiment of the same flow [48], shown in Fig. 8, can be seen to compare very favorably. As above, only low order numerical methods were used. The use of VC2 results in slightly larger (but still constant) core sizes, and essentially the same behavior.

One other illustrative example involves the Kelvin-Helmholtz instability described in Section 1.1. A simple flow was computed where initially, a 2-D stadium shaped, thin vortex sheet with zero velocity inside. This would be expected to roll up, in the zero thickness limit, into spirals. The evolution of the filtered field was computed, using VC1 on a 128x128 grid. The initial vorticity contours are shown in Figure 9. As expected, the flow becomes unstable, but soon saturates into concentrated vortices, as shown in Figure 10.

3.1.4 Boundary Layer Models

This section does not directly involve LES. However, the turbulent wakes described in Ref. [0], originate from boundary layers (BLs) separating from blunt bodies. For this reason, we describe the general use of VC for creating implicit models for these BLs. Here, VC provides a very simple, low-cost substitute for RANS models. However, it should have comparable accuracy for these applications, since the BL treatment is consistent with the VC treatment of the vortices in the wake. We describe two approaches: the use with immersed BL's, and the use with surface – conforming grids. Both enforce the necessary no-flow-through conditions. They also enforce no-slip conditions. This latter feature ensures that the resulting BL has the correct total vorticity, which is just the difference between the velocity at the outer edge of the BL and the inner velocity, which is zero. This, in turn, ensures that a separating BL has the correct total vorticity. Since VC also ensures that a separating BL will subsequently remain thin (but can still roll-up or lead to large-scale separation), this treatment should be accurate, since when the separating BL is thin, the details of the internal structure should not have an important influence. Both of these approaches involve coarse, inviscid-size grids. These models do not involve determining a detailed time-averaged velocity profile, as in RANS schemes, which would require a very fine, body-fitted grid: Instead, they models the profile over only a few coarse

grid cells. As such, they are meant to be useful for blunt body flows with massive separation, where the internal structure of this profile, as well as skin friction, are of secondary importance compared to the location and strength of the separating BL.

With a conventional CFD solution without VC, even for attached flow, the BL vorticity would quickly convect and diffuse away from the surface regions due to the large numerical errors at the boundary resulting from the coarse and possibly non-conforming grid, destroying the accuracy of the outer solution. However, the use of VC confines vorticity to 1-3 grid cells along the surface, when it is attached. Just outside this layer the velocity is smooth and close to tangent to the adjacent surface [49]. The important feature here is that an attached BL, even with constant confinement parameters, maintains a constant thickness. This is close to the very slow thickness growth ($x^{1/7}$) of physical turbulent BLs in constant pressure gradients (on flat plates). This simple boundary layer can still separate, however, especially at edges and in regions of strong adverse pressure gradient.

The VC1 version has a very simple interpretation for attached boundary layers: In this case, the vector $\hat{n}$ in Equation 3.4, as explained, is defined to be locally normal to the surface in the boundary layer region. Then, VC1 is simply a combination of positive diffusion (which spreads the vorticity away from the surface) and convection of vorticity towards the surface. This has proven to be a very robust and efficient way of modeling the boundary layer, combining a tangential smoothing for the external velocity and a "compression" of the vorticity in the normal direction.

A number of results have been presented which demonstrate the effectiveness of this approach [20-23]. In cases where the BL separates, it can be seen to remain thin because of VC. Other immersed surface methods apparently result in numerical diffusion and numerical thickening of the separating BL's [47].

a. Immersed boundary layer model

To enforce no-slip boundary conditions on immersed surfaces, first, the surface is represented implicitly by a smooth "level set" function, "F", defined at each grid point. This is just the (signed) distance from each grid point to the nearest point on the surface of an object – positive outside, negative inside. Then, at each time step during the solution, velocities in the interior are simply set to zero. In a computation using VC, this results in thin vortical region along the surface, which is smooth in the tangential direction, with no "staircase" effects.

The important point is that no special logic is required in the "cut" cells, unlike many conventional schemes: only the same VC equations are applied, as in the rest of the grid, but with a different form for $\hat{n}$. Also, unlike many conventional immersed surface schemes, which are inviscid because of cell size constraints, there is effectively a no-slip boundary condition, which results in a boundary layer with well-defined total vorticity and which, because of VC, remains thin, even after separation.

The method is especially effective for complex configurations with separation from sharp corners. Also, even with constant coefficients, it can approximately treat separation from smooth surfaces, as shown in Ref. [0].

Results (tangential velocity contours) are presented in Figs. 11 and 12, for a computation on a uniform Cartesian with 128x128 cells, for flow over an immersed, oblique flat plate in zero pressure gradient. The resulting large, diffusive numerical errors can be seen in Fig. 11, for the case with no VC. For this flow, the velocity is simply set to zero at nodes below the surface. (The small wiggles are from the spline fit in the contour plotter.) It can be seen that these are eliminated, to plottable accuracy, for the case with VC1, plotted in Fig. 12. Here, as in Sec. 3.1.3, only low order numerical methods were used with constant confinement coefficients.

b. Conforming grid boundary layer model

We are beginning to develop detailed models for turbulent boundary layers, within the VC framework. This involves modeling the evolution of the Confinement parameters so that, for example, separation is accurately predicted, even on smooth surfaces in time-dependent adverse pressure gradients. Results of some new, exploratory studies for these cases will also be described in Ref. [0]. There is still research to be done on these models, but the capabilities of the basic approach appear to be very promising.

An important point, is that this VC-based method is fundamentally different from conventional RANS schemes, which typically use an eddy viscosity (EV) type of term and discretise a (modified) Navier-Stokes type of equation on a very fine grid, in order to model the time-averaged velocity. A very important feature of VC here is that it greatly expands our modeling capability, compared to EV – type schemes: Typically, these latter schemes can only accommodate positive values of EV. If the EV is negative over significant regions of space and time, they tend to diverge due to numerical instability [36]. This means that the modeled BL can only directly be made to expand, or diffuse, and not to contract. (Of course, slower expansion rates can be obtained and smaller BL thickness, but a finer grid is then required and a smaller value of the EV.) VC, on the other hand, can directly model contraction, and,

unlike a conventional scheme with a negative eddy viscosity, VC will not diverge. This is very useful, for example, in turbulent BL separation from a smooth surface at moderate values of Re: physically, the separating layer then tends to transition and quickly reattach. A contraction term such as VC easily models this effect [37].

Another point is that, for conforming grids with variable cell sizes, a scaling factor must be applied to μ and ε which depends on this size [38]. This is not a large correction, since inviscid-size grids are used that do not have large aspect ratios.

A final point involves the use of VC in retarding separation in adverse pressure gradient regions. For example, as is well known, a turbulent BL tends to separate later (in an adverse pressure gradient) than a laminar one. VC can easily be used to simulate this by increasing the confinement strength, again without very fine grids. [20]

3.2 Comparison of the VC2 Formulation with Direction-Split Discontinuity Steepening Schemes

In this section, we describe advantages of VC over direction-split discontinuity steepening schemes. We first reformulate the one-dimensional scalar pulse equation of section 2. as a steepening method for velocity contact discontinuities. The result has some similarity to forms that have been developed over a number of years to keep gradient steep and overcome the smoothing resulting from the convection terms. As explained above, these schemes have typically involved one-dimensional compressible flows and have a number of essential differences, compared to VC.

If we consider the integral of the one-dimensional pulse of section 2. (and change the sign), we have a propagating step function that remains steep for arbitrarily long times (see Figure 13). Making the substitution:

$$\phi_j^n \equiv \delta_j V_j^n = V_j^n - V_{j-1}^n \qquad (3.10)$$

Eqn. (2.6) becomes

$$\Phi_j^n = \Phi_j^n\left(\left\{\delta_j V_j^n\right\}\right) \qquad (3.11)$$

Partially summing Equation (2.7) over j, we then have (for constant c)

$$V_j^{n+1} = V_j^n - \frac{v}{2}\left(V_{j+1}^n - V_{j-1}^n\right) + \mu \delta_j^2 V_j^n - \varepsilon \delta_j \Phi_j^n \qquad (3.12)$$

In this form Confinement is, effectively, a one-dimensional steepening scheme. However, real flows never have a single region in which they have a steep gradient, and exactly constant properties everywhere else. In general, there are O(1) (smooth) gradients away from the discontinuity region. In 1-D, these smooth gradients are also acted on by the steepener, causing errors, unless special logic is used to cut-off the steepener.

Using such one-dimensional schemes along each coordinate axis to keep a convecting vortex core compact by maintaining the steep gradients there would cause the same problem, since the velocities vary inversely with the radius away from the core (see Figure 14). However, we do not do this! The important point is that we should not use the exact one-dimensional Confinement terms, but should only keep their basic mathematical structure - that they are functions of first derivatives of velocities. In developing a formulation for multiple dimensions, we should then use only rotationally invariant quantities. The only quantities, for example in 2-D incompressible flow, which are first derivatives of a velocity are:

$$\omega = \vec{\nabla} \times \vec{q}\big|_k \text{ (3.15)}$$

and

$$D = \vec{\nabla} \cdot \vec{q} \qquad (3.16)$$

where k denotes the out-of-plane direction. But $D = 0$ for incompressible flow, so we have only one choice:

$$\Phi = \Phi(\omega). \qquad (3.17)$$

This eliminates any problems with gradients away from the core since just outside the core, $\omega \to 0$, even though both $\partial_x v$ and $\partial_y u$ are O(1) there. In addition, this choice results in a much simpler formulation than using separate operators along each axis. Finally, for a vortex filament in three-dimensions, we consider it sufficient to confine in a two-dimensional plane normal to the vortex, as depicted in Figure 15. In this way we arrive at the momentum conserving VC formulation.

4 Conclusions

A computational method is described that has been designed to capture thin vortical regions in high Reynolds number incompressible flows. The principal objective of the method—Vorticity Confinement (VC)—is to capture the *essential* features of these small-scale vortical structures and model them with a very efficient difference method

directly on an Eulerian computational grid. Effectively, the small vortical scales are treated as *nonlinear solitary waves* that "live' on the lattice indefinitely. The method allows isolated, convecting structures to be modeled over as few as 2 grid cells with no numerical spreading as they convect over arbitrarily long distances, with no special logic required for merging or reconnection. It also serves as a very efficient substitute for RANS models of attached and separating boundary layers and vortex sheets and filaments. Further, the method easily allows boundaries with no-slip conditions to be treated as "immersed" surfaces in uniform, non-conforming grids, with no requirements for complex logic involving "cut" cells.

In this paper, a description of the basic VC method is given. This is more comprehensive than has been previously available. There are close analogies between VC and well-known shock and contact discontinuity capturing methodologies. These are discussed to explain the basic ideas behind VC, since it is somewhat different than conventional CFD methods. Some of the possibilities that VC offers towards very efficient computation of turbulent flows in LES approximations are also explored. These stem from the ability of VC to act as a negative dissipation at scales just above a grid cell, but that saturates and does not lead to divergence. This feature allows

1- approximate cancellation of numerical diffusion, so that more complex, high order-low dissipation schemes can be avoided. Small-scale vortical structures at the grid cell level can then be captured, resulting in very efficient use of the available degrees of freedom on the grid.

2- approximate treatment of backscatter. This involves the addition of (modeled) subgrid kinetic energy to the flow in a natural way, without requiring stochastic forcing, and which restores some of the instabilities that are removed by the (implicit) filtering.

Although used for a number of years for complex, attached and separating flows, and trailing vortices, its use as an LES method is relatively recent.

In Ref. [0], results of initial applications of VC to LES will be presented.

5 Acknowledgements

6 References

[0] Steinhoff, J., et. al., "Computation of High Reynolds Number Flows Using Vorticity Confinement: II. Results," UTSI Preprint, March 2005.

[1] Von Neumann, J., and Richtmyer, R.D., "A Method for the Numerical Calculation of Hydrodynamic Shocks," *J. Appl. Phys.*, Vol. 21, No. 3, 1950.

[2] Lax, P. D., "Hyperbolic Systems of Conservation Laws II," *Comm. Pure Appl. Math*, Vol. 10, 1957.

[3] Harten, A., "The Artifical Compression Method for Computation of Shocks and Contact Discontinuities III, Self-Adjusting Hybrid Schemes," *Mathematics of Computation*, Vol. 32, No. 142, April 1978.

[4] Van Leer, B., "Towards the Ultimate Conservative Difference Scheme. II. Monotonicity and Conservation Combined in a Second-Order Scheme," *J. Comp. Phys.*, Vol. 14, 1974.

[5] Steinhoff, J., Senge, H., and Wenren, Y., "Computational Vortex Capturing," UTSI preprint, 1990.

[6] Steinhoff, J., Mersch, T., Underhill, D., Wenren, Y., and Wang, C., "Computational Vorticity Confinement: A Non-Diffusive Eulerian Method for Vortex Dominated Flows," UTSI preprint, 1992.

[7] Steinhoff, J., and Underhill, D., "Modification of the Euler Equations for "Vorticity Confinement" – Application to the Computation of Interacting Vortex Rings", *Physics of Fluids*, Vol. 6, August 1994.

[8] Wang, C., Steinhoff, J., and Wenren, Y., "Numerical Vorticity Confinement for Vortex-solid Body Interaction Problems", *AIAA Journal*, Vol. 33, August 1995.

[9] Steinhoff, J., Puskas, E., Babu, S., Wenren, Y., and Underhill, D., "Computation of Thin Features Over Long Distances Using Solitary Waves," AIAA Proceedings, 13th Computational Fluid Dynamics Conference, July, 1997.

[10] Steinhoff, J., Wenren, Y., and Wang, L., "Efficient Computation of Separating High Reynolds Number Incompressible Flows Using Vorticity Confinement," AIAA-99-3316-CP 1999.

[11] Wenren, Y., Fan, M., Wang, L., and Steinhoff, J., "Application of Vorticity Confinement to the Prediction of Flow over Complex Bodies", *AIAA Journal*, Vol. 41, May 2003.

[12] Steinhoff, J., Fan, M., Wang, L., and Dietz, W., "Convection of Concentrated Vortices and Passive Scalars as Solitary Waves," *SIAM Journal of Scientific Computing*, Vol. 19, December 2003.

[13] Hu, G., Grossman, B., and Steinhoff, J., "A Numerical Method for Vortex Confinement in Compressible Flow," *AIAA-Journal*, Vol. 40, October 2002.

[14] Dadone, A., Hu, G., Grossman, B., "Towards a Better Understanding of Vorticity Confinement Methods in Compressible Flow," AIAA-2001-2639. AIAA Anaheim meeting, June 2001.

[15] Dietz, W., "Application of Vorticity Confinement to Compressible Flow," AIAA-2004-0718. AIAA Reno meeting, January 2004.

[16] Costes, M., and Kowani, G., "An Automatic Anti-diffusion Method for Vortical Flows Based on Vorticity Confinement", *Aerospace Science and Technology*, Vol. 7, 2003.

[17] Wenren, Y., Steinhoff, J., and Robins, R., "Computation of Aircraft Trailing Vortices," SBIR Final Report, June 1995.

[18] Wenren, Y., Fan, M., Dietz, W., Hu, G., Braun, C., Steinhoff, J., Grossman, B., "Effeicient Eulerian Computation of Realistic Rotorcraft Flows Using Vorticity Confinement: A Survey of Recent Results," AIAA-2001-0996. AIAA Reno meeting, January 2001.

[19] Dietz, W., Fan, M., Steinhoff, J., Wenren, Y., "Application of Vorticity Confinement to the Prediction of the Flow Over Complex Bodies," AIAA-2001-2642. AIAA Anaheim meeting, June 2001.

[20] Fan, M., Wenren, Y., Dietz, W., Xiao, M., Steinhoff, J., "Computing Blunt Body Flows on Coarse Grids Using Vorticity Confinement," *Journal of Fluids Engineering*, Vol. 124, No. 4, pp. 876-885, December 2002.

[21] Steinhoff, J., Dietz, W., Haas, S., Xiao, M., Lynn, N., and Fan, M., "Simulating Small Scale Features In Fluid Dynamics And Acoustics As Nonlinear Solitary Waves," AIAA-2003-0078. AIAA Reno meeting, January 2003.

[22] Fan, M., and Steinhoff, J., "Computation of Blunt Body Wake Flow by Vorticity Confinement," AIAA-2004-0592. AIAA Reno meeting, January 2004.

[23] Dietz, W., Wang, L., Wernen, Y., Caradonna, F., and Steinhoff, J., "The Development of a CFD-Based Model of Dynamic Stall," AHS 60th Annual Forum, Baltimore, MD, June, 2004.

[24] Braun, C., "Application of Vorticty Confinement to the Flow over a 6:1 Ellipsoid at High Angles of Attack" Master thesis, Institut fur Luft- und Raumfahrt, RWTH Aachen, Germany, 2000.

[25] Boris, J., and Book, D., "Flux-Corrected Transport: I SHASTA, A Fluid Transport Algorithm That Works," *Journal of Computational Physics*, Vol. 11, 1973.

[26] Grinstein, F., and Fureby, C., "Implicit Large Eddy Simulation of High-Re Flows with Flux-Limiting Schemes," AIAA-2003-4100. AIAA Orlando meeting, June 2003.

[27] Katz, J., and Plotkin, A., *Low Speed Aerodynamics*, Cambridge University Press, New York, 2001.

[28] Tannehill, J., Anderson, D., and Pletcher, R., *Computational Fluid Mechanics and Heat Transfer*, Taylor & Francis, 1997.

[29] Steinhoff, J.; Puskas, E.; Babu, S.; Wenren, Y.; Underhill, D., "Computation of thin features over long distances using solitary waves," AIAA Proceedings, 13th Computational Fluid Dynamics Conference, pp. 743-759, 1997.

[30] Steinhoff, J., Mersch, T., Wenren, Y., "Computational Vorticity Confinement: Two Dimensional Incompressible Flow," *Developments in Theoretical and Applied Mechanics*, Proceedings of the Sixteenth Southeastern Conference on Theoretical and Applied Mechanics, 1992.

[31] Bohr, T., Jensen, M., Paladin, G., and Vulpiani, A., *Dynamical Systems Approach to Turbulence*, Cambridge, 1998.

[32] Melander, M. V., McWilliams, J. C., and Zabusky, N.J., "Axisymmetrization and Vorticity-gradient Intensification of an Isolated Two-dimensional Vortex through Filamentation," *Journal of Fluid Mechanics*, Vol. 178, 1987.

[33] Misra, A., Pullin, D., "A Vortex-based Stress Model for Large-eddy Simulation," *Physics of Fluids*, Vol. 9, No. 8, August 1997.

[34] Kim, J., and Moin, P., "Application of a Fractional-Step Method to Incompressible Navier-Stokes Equations," *Journal of Computational Physics*, Vol. 59, No. 2, 1985.

[35] Steinhoff, J., Fan, M., and Wang, L., "Vorticity Confinement – Recent Results: Turbulent Wake Simulations and a New, Conservative Formulation," *Numerical Simulations of Incompressible Flows*, Ed. By M. M. Hafez, World Scientific, 2003.

[36] Ferziger, J., "Large Eddy Simulation," *Simulation and Modeling of Turbulent Flows*, Ed. By T. B. Gatski, M.Y. Hussaini and J.L. Lumley, Oxford, 1996.

[37] Dietz, W., "Analysis, Design, and Test of Low Reynolds Number Rotors and Propellers," SBIR Final Report, September 2004.

[38] Steinhoff, J., and Raviprakash, G., "Navier-Stokes Computation of Blade-Vortex Interaction Using Vorticity Confinement," AIAA-95-0161. AIAA Reno meeting, January 1995.

[39] Haas, S., "Computation of Trailing Vortex Flow Over Long Distances Using Vorticity Confinement," Master thesis, Institut fur Luft- und Raumfahrt, RWTH Aachen, Germany, 2003.

[40] Dietz, W., Wenren, Y., Wang, L., Chen, X., and Steinhoff, J., "Scalable Aerodynamics and Coupled Comprehensive Module for the Prediction of Rotorcraft Maneuver Loads," SBIR Final Report, May 2004.

[41] Szydlowski, J., and Costes, M., "Simulation of Flow Around a NACA0015 Airfoil for Static and Dynamic Stall Configurations Using RANS and DES," 4th Decennial Specialist's Conference on Aeromechanics, January 2004.

[42] Fedkiw, R., Stam, J., and Jensen, H. W., "Visualizations of Smoke", Proceedings of SIGGRAPH 2001, Los Angeles, 2001.

[43] Robinson, M., "Application of Vorticity Confinement to Inviscid Missile Force and Moment Prediction," AIAA-2004-0717. AIAA Reno meeting, January 2004.

[44] Suttles, T., Landrum, D., Greiner, B., and Robinson, M., "Calibration of Vorticity Confinement Techniques for Missile Aerodynamics:
Part I - Surface Confinement," AIAA-2004-0719. AIAA Reno meeting, January 2004.

[45] Morvant, R., Badcock, K., Barakos, G., and Richards, B., "Aerofoil-Vortex Interaction Simulation Using the Compressible Vorticity Confinement Method," 29th European Rotorcraft Forum, Friedrichshafen, Germany, September 2003.

[46] Morvant, R., "The Investigation of Blade-Vortex Interaction Noise Using Computational Fluid Dynamics," PhD Dissertation, University of Glasgow, United Kingdom, February 2004.

[47] Mittal, R., Iaccarino, G., "Immersed Boundary Methods," *Annual Review of Fluid Mechanics*, Vol. 37, Ed. By Lumley, J., Davis, S., and R. Moin, Annual Reviews Press, 2005.

[48] Y. Oshima and N. Izutsu, "Cross-linking of two vortex rings," *Physics of Fluids*, Vol. 31, 1988.

[49] Proceedings 4th ARO Workshop on Vorticity Confinement, UTSI, November 2000.
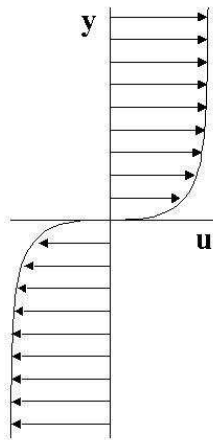
Figure 1. Velocity profile–filtered shear layer
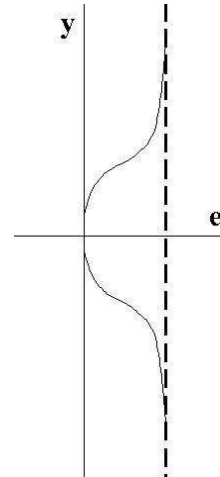
Figure 2. Energy profile–filtered and unfiltered shear layer
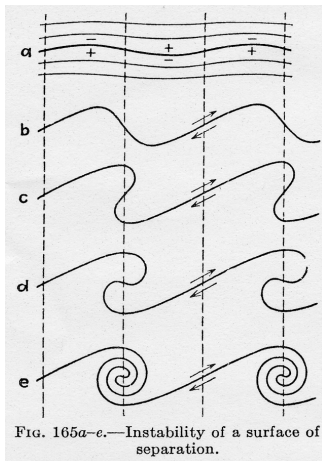
FIG. 165a–e.—Instability of a surface of separation.

Figure 3. Kelvin-Helmholtz Instability
Prandtl & Tietjens: *Fundamentals of Hydro-
and Aeromechanics*, Dover, New York, 1934.
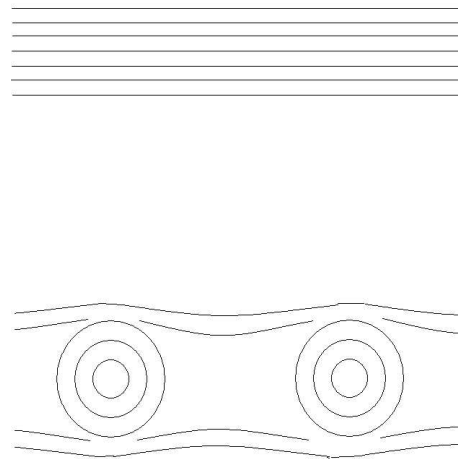
Figure 4. Vorticity contours – filtered shear layer

With Confinement
< 1 Pass
(900 Timesteps)

With Confinement
100 Passes
(110900 Timesteps)

Without Confinement
1/10 Pass
(100 Timesteps)
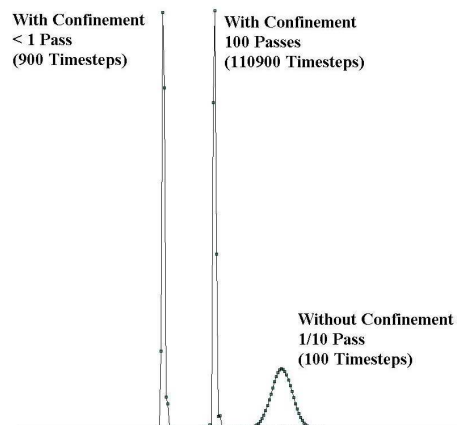
Figure 5. One-dimensional scalar convection with and without Confinement.
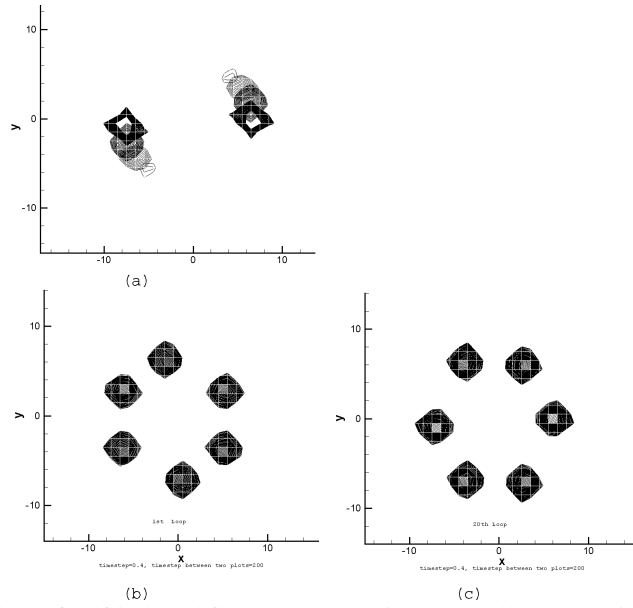
Figure 6. Vorticity contour plots of self-induced flow by two vortices (14 cells apart) with same sign (a) without vorticity confinement; (b) with vorticity confinement, 1st loop; (c) with vorticity confinement, after 20 loops.
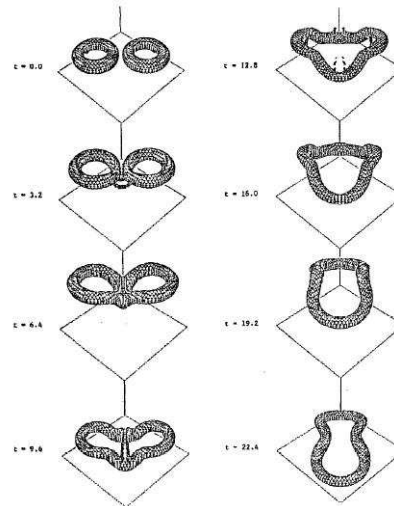
Figure 7. Coplanar Vortex Rings – Computation
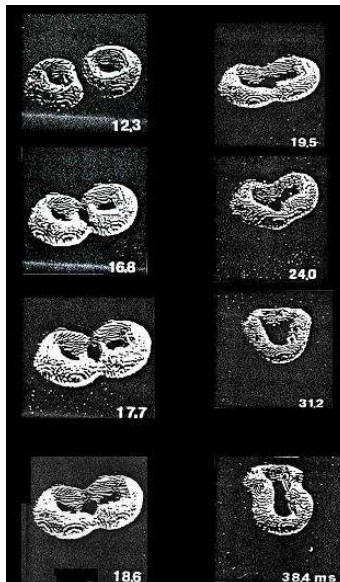
Figure 8. Coplanar Vortex Rings – Experiment (Ref. [48])
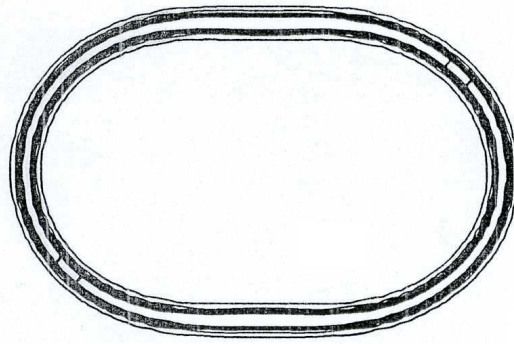
Figure 9. Initial Vorticity Contours of Two Dimensional Computation
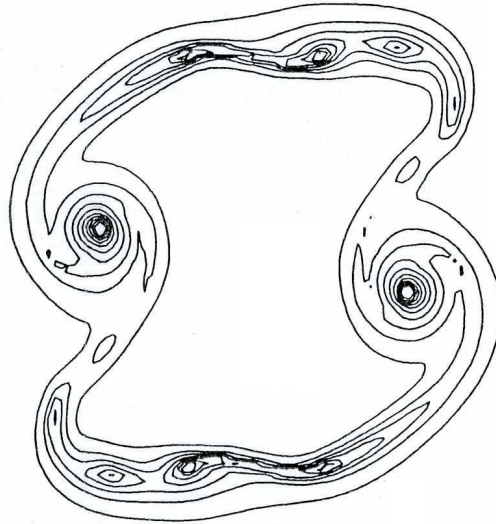
Figure 10. Vorticity Contours Showing Instability and Formation of Concentrated Vortices
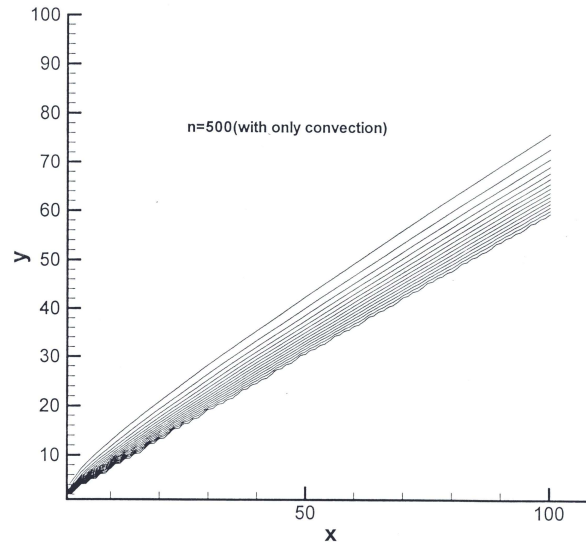
Figure 11. Immersed Surface without Vorticity Confinement
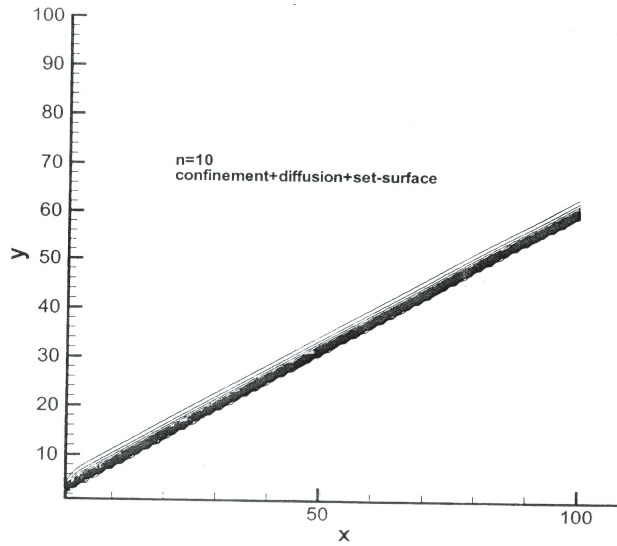
Figure 12. Immersed Surface with Vorticity Confinement
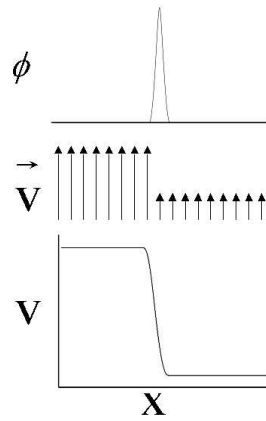
Figure 13. Comparison between 1-D discontinuity capturing schemes and pulse advection.
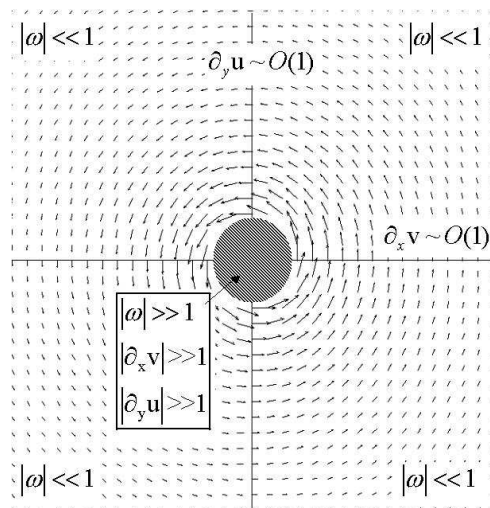
Figure 14. Velocity vector field around a vortex displaying the basis of choosing a rotationally invariant steepener.

$\vec{\omega}$

Normal Plane
- Induced
Velocity
Field
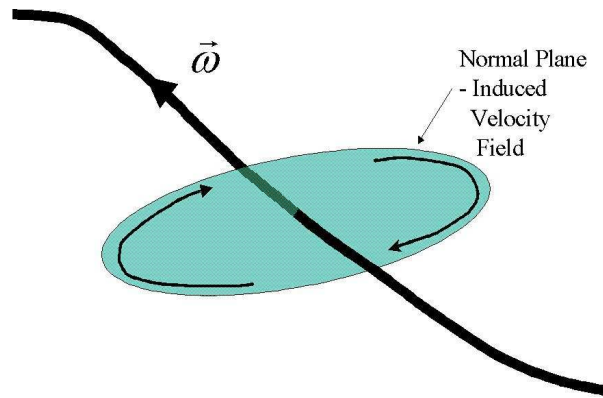
Figure 15. Confinement operator in three dimensions

Computation of High Reynolds Number Flows Using Vorticity Confinement: II. Results

John Steinhoff[4], Nicholas Lynn[5], Wenren Yonghu[6], Meng Fan[7], Lesong Wang[8], and Bill Dietz[9]

1 Introduction

In Ref. [0], as explained in the abstract, a computational method is described that has been designed to capture thin vortical regions in high Reynolds number incompressible flows. In that paper a description of the basic VC method was given.

The important point is that VC, even in its simplest "*zeroth* order" form with constant coefficients, on a coarse grid, can capture most of the main features of high Reynolds number flows. This is mainly because VC involves, in addition to a positive eddy-type viscosity, a *negative* one that does not diverge, but automatically saturates. This allows a much simpler turbulence modeling approach. Further, arguments (presented in Ref. [0]) show that just such a negative viscosity should be required: Even with *no* numerical dissipation issues, to accurately simulate a filtered field, in certain regions of the flow a term should be added to the Euler equations that acts like such a negative dissipation with saturation.

In Ref. [0] two VC formulations were described: VC1 and VC2, which involve first and second order derivatives, respectively. VC1 converges more rapidly. The main difference is that VC1 closely conserves momentum, while VC2 explicitly conserves it, making the latter more accurate for computations of vortex trajectories over long distances. In this paper, some sample results are presented from recent computations for both formulations.

We feel that for turbulent flows, computed surface pressures or mean velocities are not sufficient to describe the flow: The entire field should have vortical scales that are small enough to allow reasonable resolution. For this reason, and to get an understanding of the basic features of VC, we present visualizations of the vorticity in the field for several computations.

Of course, detailed plots of pressure or velocity are presented for a number of cases. However, if the qualitative properties of the main flow field are not correct, we feel that the validation is not complete.

2 Results

2.1 Ellipsoid

Flow over a blunt body is of considerable interest in CFD, as these flows are characterized by large-scale separation that is difficult and costly to simulate using conventional CFD methods. The Vorticity Confinement method (VC1 formulation) was used to compute the flow over a 6:1 ellipsoid for several angles of attack. Fig. 1 depicts the body embedded in a coarse uniform Cartesian grid ($188 \times 70 \times 100$). The length of the ellipsoid was 120 cells and the diameter 20 cells.

The configuration was also run with a conventional incompressible finite-volume Navier-Stokes flow solver (with a k-ε turbulence model) using body-fitted structured grids (Ref. [1]). Comparisons between the Vorticity Confinement results, experiment, and the conventional flow solver (designated as F-V) for 20 degrees and 25 degrees angle of attack are reproduced in Fig. 2. At these high angles of attack, the flow is characterized by large-scale separation and the development of steady vortical structures on the lee side of the configuration. In both cases, the Vorticity Confinement results agree well with experiment and the F-V computation. Use of non-body-conforming Cartesian grids eliminates any difficulties with grid generation, and the use of Vorticity Confinement allows results to be obtained on much coarser meshes than is possible with conventional Navier-Stokes grids. The Vorticity Confinement calculations required about 5 hours on a Pentium II-class computer.

An important point is that these comparisons involve surface pressure, for which the body-fitted grid was optimized. Unlike the conventional method, the VC method did not lose resolution in the wake, since it used a uniform Cartesian grid. Resolving the wake is often an important goal in computing these flows (such as for submarines).

---

[4] Professor, The University of Tennessee Space Institute, Tullahoma, TN
[5] Graduate Research Assistant, The University of Tennessee Space Institute, Tullahoma, TN
[6] Research Scientist, Flow Analysis, Inc.
[7] Research Scientist, The University of Tennessee Space Institute, Tullahoma, TN
[8] Research Scientist, Flow Analysis, Inc.
[9] Research Scientist, Flow Analysis, Inc.

2.2 Jet Pulme

A jet plume was computed issuing from a flat plane at an angle of 30 degrees. There was no crosswind velocity. Two cases were computed, one without Vorticity Confinement, and another with the VC1 formulation. In the case without VC, shown in Figure 3, the smallest scales quickly dissipate. VC resolves the smaller structures on the computational grid, as seen in Figure 4. The computational grid was $129 \times 65 \times 65$, and the computational time was less than 30 minutes for 300 time steps, for a 1.8 GHz Pentium processor with 1 GB of memory.

2.3 Forced Turbulence

Computations for 3-D randomly stirred turbulence were done using the VC1 formulation. A coarse, uniform Cartesian grid of the dimensions $64 \times 64 \times 64$ was used with periodic boundary conditions. The CFL number for the computation was 0.2.

Forcing was added every time step for the first ten-thousand time steps:

$$\hat{u}_x = A\left[\partial_y \phi_3 - \partial_z \phi_2\right]$$
$$\hat{u}_y = A\left[\partial_z \phi_1 - \partial_x \phi_3\right]$$
$$\hat{u}_z = A\left[\partial_x \phi_2 - \partial_y \phi_1\right]$$

where A is a constant, and ϕ_1, ϕ_2 and ϕ_3 are potential functions with the following expressions:

$$\phi_1 = \alpha_0 \sin\left[2\pi x/L_x + \alpha_1\right]\sin\left[2\pi y/L_y + \alpha_2\right]\sin\left[2\pi z/L_z + \alpha_3\right]$$
$$\phi_2 = \beta_0 \sin\left[2\pi x/L_x + \beta_1\right]\sin\left[2\pi y/L_y + \beta_2\right]\sin\left[2\pi z/L_z + \beta_3\right].$$
$$\phi_3 = \gamma_0 \sin\left[2\pi x/L_x + \gamma_1\right]\sin\left[2\pi y/L_y + \gamma_2\right]\sin\left[2\pi z/L_z + \gamma_3\right]$$

Here, α_0, α_1, α_2, α_3, β_0, β_1, β_2 and β_3 are random numbers generated every time step, x, y and z are coordinates, and L_x, L_y and L_z are the overall lengths of the computational grids in each direction as denoted by the subscripts.

The results presented include the compensated energy spectrum at several times and the isosurface of the vorticity field at one time. Fig. 5 shows the compensated energy spectrum of the fully developed turbulence, and the spectrum after turning the forcing off for a sufficiently long period until the turbulence fully decays. The energy spectrum is plotted using a log scale in both the wavenumber and energy (K and E, respectively) axis, and the energy was multiplied by $K^{5/3}$, so that the spectrum curve should appear flat according to the Kolmogorov theorem. For reference, the spectrum of the forcing function after one single time step was also plotted in the figure. Fig. 6 shows the vorticity isosurface for the fully developed turbulence field at time step 8,000.

2.4 Circular Cylinder

The computation of flow around a circular cylinder has been done using both the VC1 and VC2 formulations. In both cases, $\text{Re} = 3900$. A coarse, uniform Cartesian grid $181 \times 121 \times 61$ was used with an immersed boundary for the cylinder that was only 15 cells in diameter. The results presented here are from the VC2 study, although the VC1 formulation shows no significant difference (results for the VC1 formulation can be found in Ref. [2]). Both VC formulations compared very well with each other and with experiment.

Results for the VC2 formulation are presented below: Vorticity magnitude isosurfaces are shown in Fig. 7, where the isosurface magnitude has a value of ¼ of the maximum. Plots corresponding to computed average streamwise velocity along lines behind the cylinder are shown in Fig. 8 and rms streamwise velocity fluctuations are presented in Fig. 9. The lines where the measurements were taken are shown in Fig. 10. Good agreement with experiment is seen. The pressure distribution on the cylinder surface also compares very well with experiment data, as can be seen in Fig. 11.

The important point here is that only by adjusting one parameter ε, which was constant throughout the field, the computed results agreed closely with experiment for all six curves plotted in Figs. 8 and 9. Additional comparisons with experiment at different Reynolds number will be required to calibrate the Reynolds number dependence of this parameter.

It must be emphasized that the instabilities and chaotic behavior that result when ε is increased are only from three-dimensional effects, as in physical turbulence, and are not due to numerical instabilities: Extensive studies have been done over a much wider range of ε values than that studied here for flows in 2-D, where no instabilities were expected. These only showed stable flow. These studies involved vortices shedding from a two-dimensional cylinder with pairing. Other studies involved isolated, shed wing-tip vortices in three-dimensions.

2.5 Square Cylinder

Flow over a square cylinder was also calculated. As in the circular case, the cylinder was "immersed" in a uniform $141 \times 101 \times 61$ Cartesian grid and periodic conditions were imposed at the lateral boundaries. The diameter (length of each side) of the cylinder was also 15 grid cells. The same coordinate system was used as for the circular cylinder. As shown in Figure 12, results of the computations were compared to the experimental results of Lyn, et al. [3] at a Reynolds number of about 21,400. The computational results were all averaged over the spanwise direction.

As in the circular case, the diffusion coefficient, μ, and the confinement coefficient, ε, were held constant throughout the field. The confinement coefficient, ε, was adjusted to impose different levels of confinement so as to approximate the effects of different Reynolds numbers. Figure 13 depicts the comparison with experimental data of the time-averaged streamwise velocity along a streamwise line extending downstream from the middle of the leeward face of the cylinder. Results for one value of the confinement coefficient are plotted. Figure 14 shows the time-averaged velocity along a line normal to the cylinder axis and the mean stream at x = 1. Symbols represent the experimental data. The numerical results can be seen to agree well with the experimental data. Comparisons of the computed streamwise RMS velocity fluctuations with the experimental results also show good agreement in Fig. 15.

2.6 Disk

Computations were done on a 185×101×101 uniform Cartesian grid. The disk diameter and width were 30 and 1 grid cells, respectively. The CFL number was set equal to 0.25. The entire computation took about 52 hours on a single 933 MHz Pentium 3 processor for a nondimensional time of over 90.

The computed wake was visualized by vorticity isosurfaces of roughly 25% of maximum. These are shown for six nondimensional times, T = 2.5, 5, 10, 20, 40 and 80, in Fig 16. It can be seen that the flow resulted in instabilities and streamwise vorticity. This is very close to visualizations from wind tunnel experiments as shown in Figs. 2 and 3(a) of Ref. [4]. For comparison, vorticity isosurfaces from a computation using a conventional difference scheme are shown in Fig. 2 of Ref. [5]. The large unphysical effects of numerical diffusion are evident there. These unphysical effects also occur in our code when we turn off confinement.

The drag coefficient history for the entire computational time is shown in Fig. 17. This is very close agreement to available experimental data (Fig. 4 of Ref. [6]), and other computational results (Fig. 20 of Ref [6]).

2.7 Dynamic Stall – NACA 0015

The "TURNS" code was modified to include Vorticity Confinement. This code is compressible, but the Vorticity Confinement was implemented in a similar way as described in Ref. [0] (see Ref. [7] for more details). However, the results presented here are for a Mach number of .3, so that compressibility effects are small. The computational grid cell sizes were close to those in typical inviscid computations, even though the results are for a high Reynolds number viscous case (see Fig. 18). Traditional RANS schemes would require 2-3 orders of magnitude smaller cells near the surface and corresponding longer computing times. Vorticity Confinement (VC1) allows the no-slip condition to be satisfied, such that the boundary layer remains attached until the correct separation point. The computation required only 6,500 grid cells.

Figure 19 depicts lift and moment loops for the NACA0015 airfoil (11º < a < 19º, reduced frequency = 0.1, M = 0.3). The stall-induced moment is only moderately larger than experiment (compared to conventional CFD methods). The lift is fairly well predicted with the exception of a small region during the early downswing. The predicted moments for this case are fairly close to the data, with the exceptions of somewhat underpredicting the moment peak and the occurrence of another peak in the early downswing. The computed early downswing is marked (for this case) by the occurrence of a second vortex eruption - which is not apparent in the data.

A higher reduced frequency is shown in Figure 20 (for 13º < a < 21º, reduced frequency = 0.13, M = 0.3). In this case, it appears that the actual flow is always at least partially separated (to judge by the lift difference seen on the upswing). However, the moment comparison is not unreasonable. For this case, the moment peak is somewhat overpredicted. The accuracy of the comparisons seen in Figures 19 and 20 is close to what is required for an engineering model—especially considering the computation time, which is of the order of a minute on a PC for a single cycle.

2.8 Comanche

The flow about a realistic helicopter body (Comanche) was computed. Rotating shanks were included in the computation since they could have a significant effect on the flow behind the pylon. However, the resolution of the shank geometry should be consistent with that of the vortices which they shed, which are spread over only about 4 grid cells. Accordingly, a simple analytic representation was used for the shanks (as opposed to the main body, which was represented by surface points). The shank and body definitions were then used to compute the geometry—defining level set function for the flow computation (see Ref. [0]).

A simple uniform Cartesian grid was used in the computation which had 288x64x128 in the streamwise, horizontal and vertical directions, respectively. Figure 21 shows the pressure distribution on the body surface at one time. It can be seen in Figure 22 that strong concentrated vorticity is shed form the pylon. This will cause strong pressure fluctuations on the tail, which is seen in the experiment. In fact, a 5-per-revolution oscillating pressure was computed that corresponded closely to flight test data. Although only 3 revolutions were computed and more are required to get better statistics, good agreement in the comparison of power spectra can be seen in Figure 24. This computation was preformed on a PC (Intel Pentium II, 266 MHz, 256 MB RAM) and required 6 hours per revolution. These Comanche results were initially shown in Ref. [8]. The flight test power spectra in Figure 24 are also shown in Ref. [9]. (The power spectrum results were computed by Ted Meadowcraft of Boeing, Philadelphia.)

2.9 Missile

Computations have been performed around an unpowered missile. Vorticity Confinement was implemented as a subroutine in the "OVERFLOW-2" code. Since this computation was supersonic, a different version of VC2 (described in Ref. [10]) was used. Vorticity Confinement is used because it can capture the essential features of the separating boundary layer—maintaining its small thickness and correct circulation. Further, Vorticity Confinement allows coarse inviscid-sized grids (yet still maintains the no-slip condition at the surface) and can convect the separated vortices downsteam in a computationally efficient manner. The only other accurate alternative is the much more expensive RANS approach, since conventional, economical inviscid approaches lead to inaccurate boundary layers and expansion fans.

Normal forces and pitching moment versus angle of attack are shown in Figures 25 and 26 for a Mach number of 1.2. For a non-symmetric (three-fin) configuration, it is expected that the force and moment curves will be non-symmetric, as the proximity of the side fins to vortices shed from the body depends on the angle of attack. Very good agreement is found between the Vorticity Confinement computation and experiment. The physical asymmetries apparent in the experiment are replicated in the computation for both normal force and moment. Results at higher Mach numbers are shown in Ref. [10].

Figure 27 depicts the missile at high angle of attack in supersonic (M=1.2) flow. Missiles at high angle of attack are characterized by two main types of vortical structures: a vortex pair generated near the nose of the missile, and vortical structures generated on lifting surfaces such as fins. Physically, these structures may interact and merge while convecting downstream and have a profound impact on any downstream body. To demonstrate the need for Vorticity Confinement, cases were run with and without confinement for comparison. Without Vorticity Confinement, the vortices dissipate almost immediately and persist only slightly downstream of the missile tail, as seen in Figure 27 (a). Figure 27 (b) depicts the isosurfaces when confinement is applied. With Vorticity Confinement, the vortices persist almost indefinitely, and are free to interact with each other and any downstream object in a physically consistent manner. The capability to model the wake vortices can be critical for multiple configurations. Without confinement, the resolution of the wake vortices would require dense grids and a large number of grid points, with attendant large computational resources. It can be seen that Vorticity Confinement provides a means of capturing these structures without resorting to fine meshes.

2.10 Other Studies

The three cases presented above demonstrate uses of VC for simulating selected phenomena. Out of the large number of results obtained in the last several years, two additional results should be mentioned because they are recent and demonstrate additional uses of VC—vortex propagation and interaction with an airfoil (blade vortex interaction) and simulation and visualization of turbulent flow (for special effects). Some recent results can be seen at http://www.flowanalysis.com.

2.10.1 Blade Vortex Interaction (BVI)

The ability of VC to economically simulate propagation of concentrated vortices for BVI has made possible a recent parametric study of two-dimensional BVI cases [11, 12]. This study also utilized a compressible version of Vorticity Confinement. In these papers, it is also demonstrated that there is excellent agreement between the computations and experiment.

2.10.2 Turbulent Flow Simulations for Special Effects

For special effects, the important aspect of a turbulent simulation is, of course, that it look turbulent, which means that it include visible small scale effects. Of course this, by itself, is not sufficient for engineering purposes, but can be thought of as a prerequisite, especially if small scale phenomena are important in the problem. VC1 has been found to simulate small scale phenomena more effectively and economically than other schemes. Ron Fedkiw has performed excellent computations and visualizations with this as a goal [13].

3 Conclusion

The Vorticity Confinement (VC) method has been presented in more comprehensive detail (in Ref. [0]) than has been previously available. Although the basic ideas are somewhat different than conventional CFD, there is some commonality with a number of well-known computational methods, such as shock-capturing. Extensive use of analogies with these methods is made to explain the basic motivation.

The main goal of VC is to efficiently compute complex high Reynolds number incompressible flows, including blunt bodies with extensive separation and shed vortex filaments that convect over long distances. Almost all of the vortical regions in these flows are turbulent. This means that, for any feasible computation, they must be modeled. The remainder of the flows is irrotational and is defined once the vortical distributions are. Further, these vortical regions are often very thin.

For these reasons, the basic approach of VC is to efficiently model these regions. The most efficient way to do this appears to be to develop model equations *directly* on the computational grid, rather than to first develop model partial differential equations (pde's) and then attempt to accurately discretize them in these very thin regions.

These goals are easily achieved in the large number of flows where the essential features of the main flow are not sensitive to the internal structure of thin vortical regions. Then, VC can easily be used to capture these regions over only a

couple of grid cells and propagate them, essentially as nonlinear solitary waves that "live" on the computational lattice. Flows with these features, that are treatable with the present state of VC, include blunt bodies with separation from edges and other well-defined locations. These configurations include complex geometries that can be easily "immersed" in uniform Cartesian grids using VC. These flows also include vortex filaments which can convect, with no numerical spreading, even over arbitrarily long times, and which can merge automatically with no requirement for special logic. Flows that involve separation from smooth surfaces, and which depend on the turbulent state of the boundary layer, require more detailed modeling, including parameter calibration. This is an area of current investigation.

By contrast, a large amount of effort has been expended over a number of years by a large number of workers to develop and calibrate turbulent pde-based models for conventional eddy viscosity-based CFD schemes, such as RANS and LES. These schemes can be quite complex and can require very fine grids. The important point is that VC, even in its simplest "*zeroth* order" form with constant coefficients, on a coarse grid, can capture most of the main features of high Reynolds number flows. This is mainly because VC involves, in addition to a positive eddy-type viscosity, a *negative* one that does not diverge, but automatically saturates. This allows a much simpler turbulence modeling approach. Further, arguments (presented in Ref. [0]) show that just such a negative viscosity should be required: Even with *no* numerical dissipation issues, to accurately simulate a filtered field, in certain regions of the flow a term should be added to the Euler equations that acts like such a negative dissipation with saturation.

Preliminary results, some of which are presented, suggest that very large computer savings can be achieved, even with the simplest form of VC.

4 References

[0] Steinhoff, J., Lynn, N. and L. Wang, "Computation of High Reynolds Number Flows Using Vorticity Confinement: I. Formulation," UTSI Preprint, March 2005.

[1] Tsai, C. Y., and Whitney, A. K., "Numerical Study of Three-Dimensional Flow Separation for a 6:1 Ellipsoid," AIAA Paper no. 99-0172, 1999.

[2] Fan, M., Wenren, Y., Dietz, W., Xiao, M., Steinhoff, J., "Computing Blunt Body Flows on Coarse Grids Using Vorticity Confinement", Journal of Fluids Engineering, **124**, No. 4, pp.876-885, Dec. 2002.

[3] Lyn, D. A., Einav, S., Rodi, W., and Park, J.H., "A Laser-Doppler Velocimetry Study of Ensemble-Averaged Characteristics of the Turbulent Near Wake of a Square Cylinder ", *J. Fluid Mech.*, **304**, pp. 285-319, 1995.

[4] Berger, E., Scholz, D., and Schumm, M., "Coherent Vortex Structures in the Wake of a Sphere and a Circular Disk at Rest and Under Forced Vibrations", *Journal of Fluids and Structures*, **4**, 1990, pp.231-257.

[5] Johari, H., Stein, K., "Temporal Evolution of the Wake of an Impulsively Started Disk", FEDSM2000-11170, Proceeding of FEDSM'2000, 2000 ASME Fluids Engineering Summer Conference, June 11-15, 2000, Boston, Massachusetts.

[6] Johari, H., Stein, K., "Near Wake of an Impulsively Started Disk", *Physics of Fluids*, **14**, No. 10, 2002, pp. 3459-3474.

[7] Dietz, W., Wenren, Y., Wang, L., Chen, X., and Steinhoff, J., "Scalable Aerodynamics and Coupled Comprehensive Module for the Prediction of Rotorcraft Maneuver Loads," SBIR Final Report, May 2004.

[8] Steinhoff, J., et. al., "Proceedings," in 3rd Annual ARO Workshop on Vorticity Confinement and Related Methods, Nov. 1998.

[9] Duque, E. and Meadowcraft, E., "Numerical Evaluation of Main Rotor Pylon Flowfields on the RAH-66 Comanche Helicopter," in Proceedings, the AHS 55th Annual Forum and Technology Display, May 1999.

[10] Dietz, W., "Application of Vorticity Confinement to Compressible Flow," AIAA Paper Presented at 2004 Reno Meeting, AIAA 2004-0718.

[11] Morvant, R., Badcock, K., Barakos, G., and Richards, B., "Aerofoil-Vortex Interaction Simulation Using the Compressible Vorticity Confinement Method," 29th European Rotorcraft Forum, Friedrichshafen, Germany, September 2003.

[12] Morvant, R., "The Investigation of Blade-Vortex Interaction Noise Using Computational Fluid Dynamics," PhD Dissertation, University of Glasgow, United Kingdom, February 2004.

[13] Fedkiw, R., Stam, J., and Jensen, H. W., "Visualizations of Smoke", Proceedings of SIGGRAPH 2001, Los Angeles, 2001.

[14] Norberg, C., "Effects Of Reynolds Number And Low-intensity Freestream Turbulence On The Flow Around A Circular Cylinder", *Department of Applied Thermodynamics and Fluid Mechanics, Chalmer University of Technology*, *Sweden Rep*. **87** (2), 1987.

5 Figures
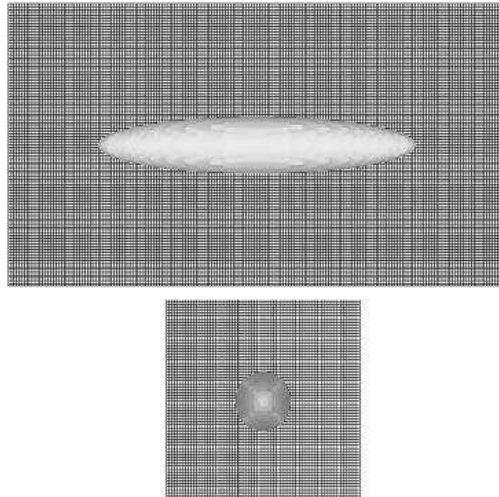
Figure 1. Ellipsoid Embedded in Uniform Grid

a) x/L = 0.77, α = 20^0

b) x/L = 0.77, α = 25^0
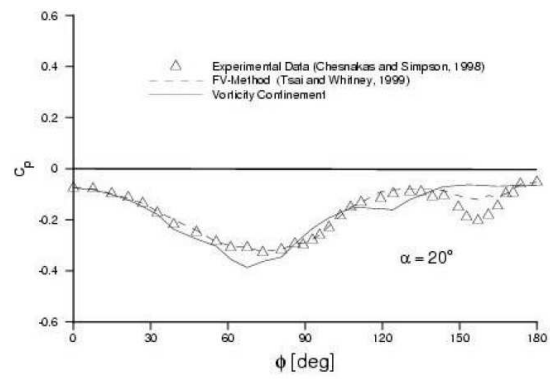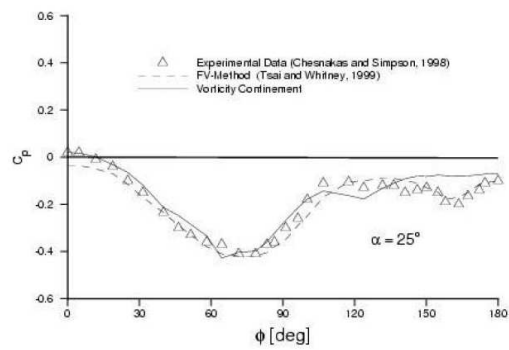
Figure 2. Comparison of Experimental and Computed Pressure Coefficients for Ellipsoid.
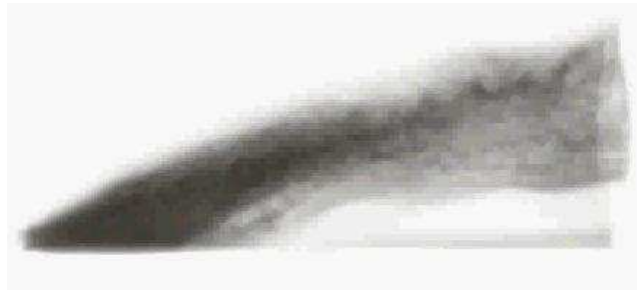
Figure 3. Jet Plume Without Vorticity Confinement

Figure 4. Jet Plume With Vorticity Confinement
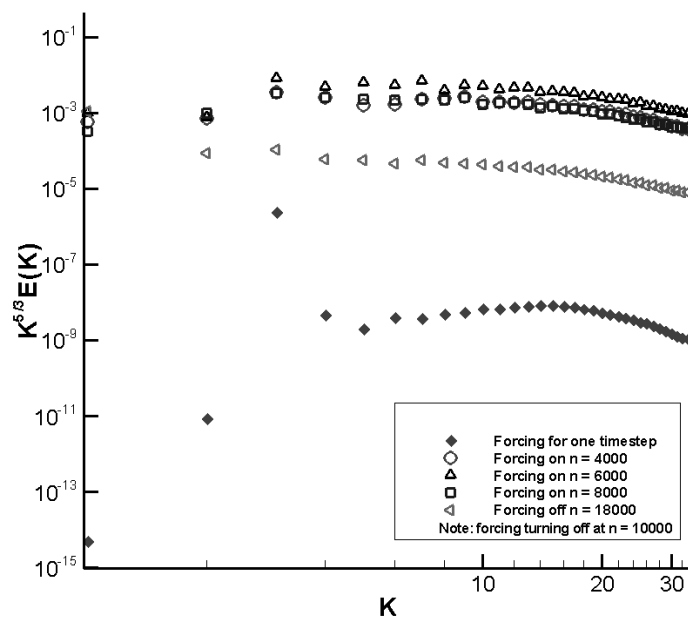
Figure 5. Compensated Energy Spectrum
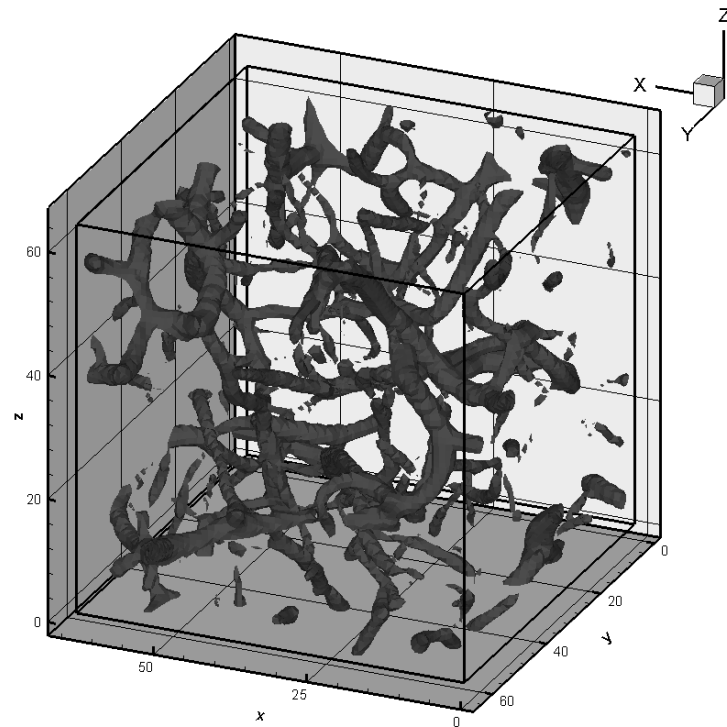
Figure 6. Vorticity Isosurface at 8000th Timestep
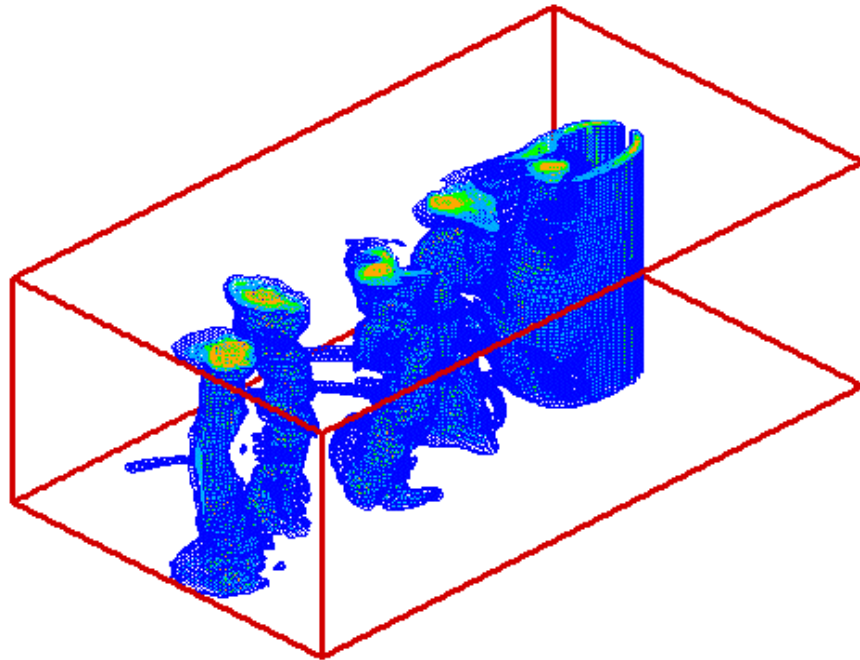
Figure 7. Vorticity Isosurface for Flow over Cylinder with Vorticity Confinement ($\mu = 0.15, \varepsilon = 0.325$)
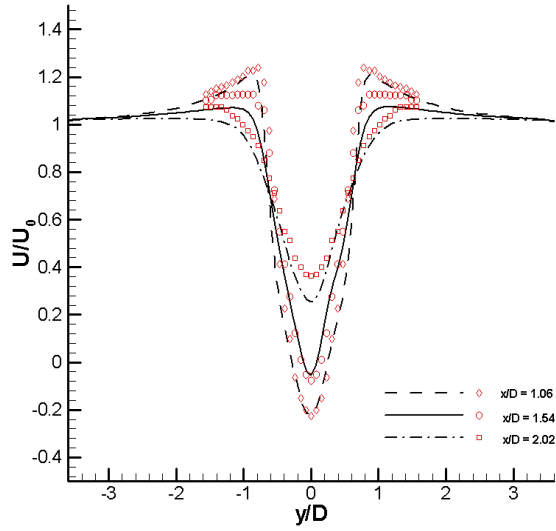
Figure 8. Mean Streamwise Velocity Profiles. Symbols are Experimental Data ($\mu = 0.15, \varepsilon = 0.325$)
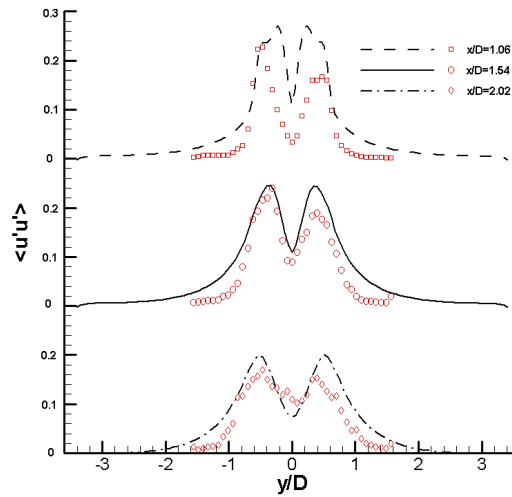
Figure 9. Streamwise Reynolds stresses. Symbols are Experimental Data ($\mu = 0.15, \varepsilon = 0.325$)
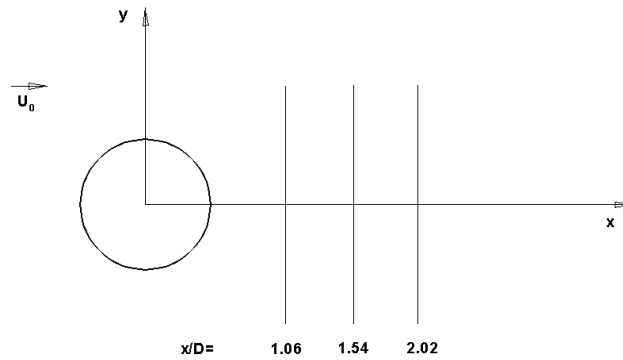
Figure 10. Measurement Positions For Circular Cylinder
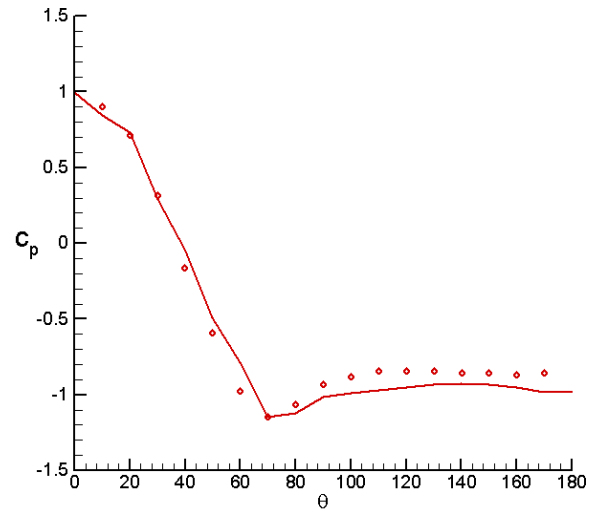
Figure 11. Time-averaged Pressure Coefficient Distribution on the Cylinder Surface. Circles Denote Experimental Data of Norberg ([14], 1987)
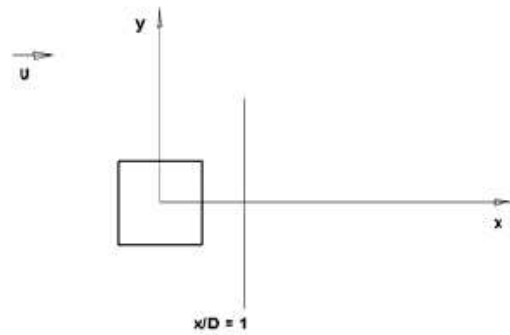
Figure 12. Measurement Position for Square Cylinder
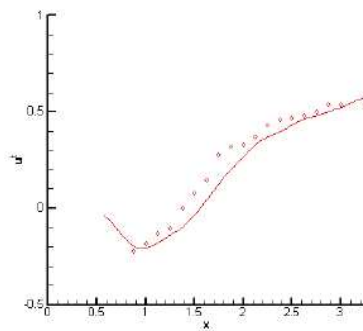
Figure 13. Comparison of time-averaged streamwise velocity along a streamwise line. Symbols denote experimental data.
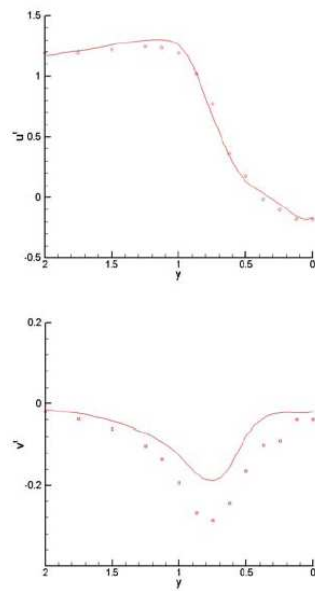
Figure 14. Comparison of time-averaged velocity profiles at x = 1. Symbols are experimental data.
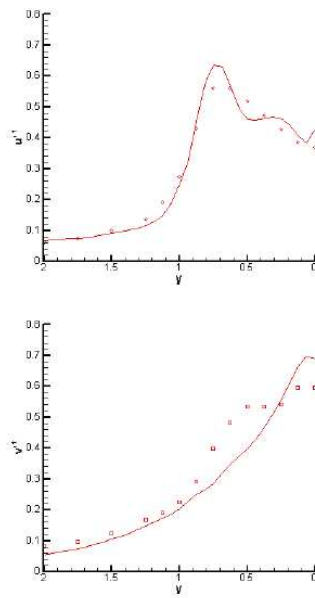
Figure 15. Comparison of root mean square velocity fluctuation profiles at x = 1. Symbols are experimental data.

(a)

(b)

(c)

(d)

(e)

(f)
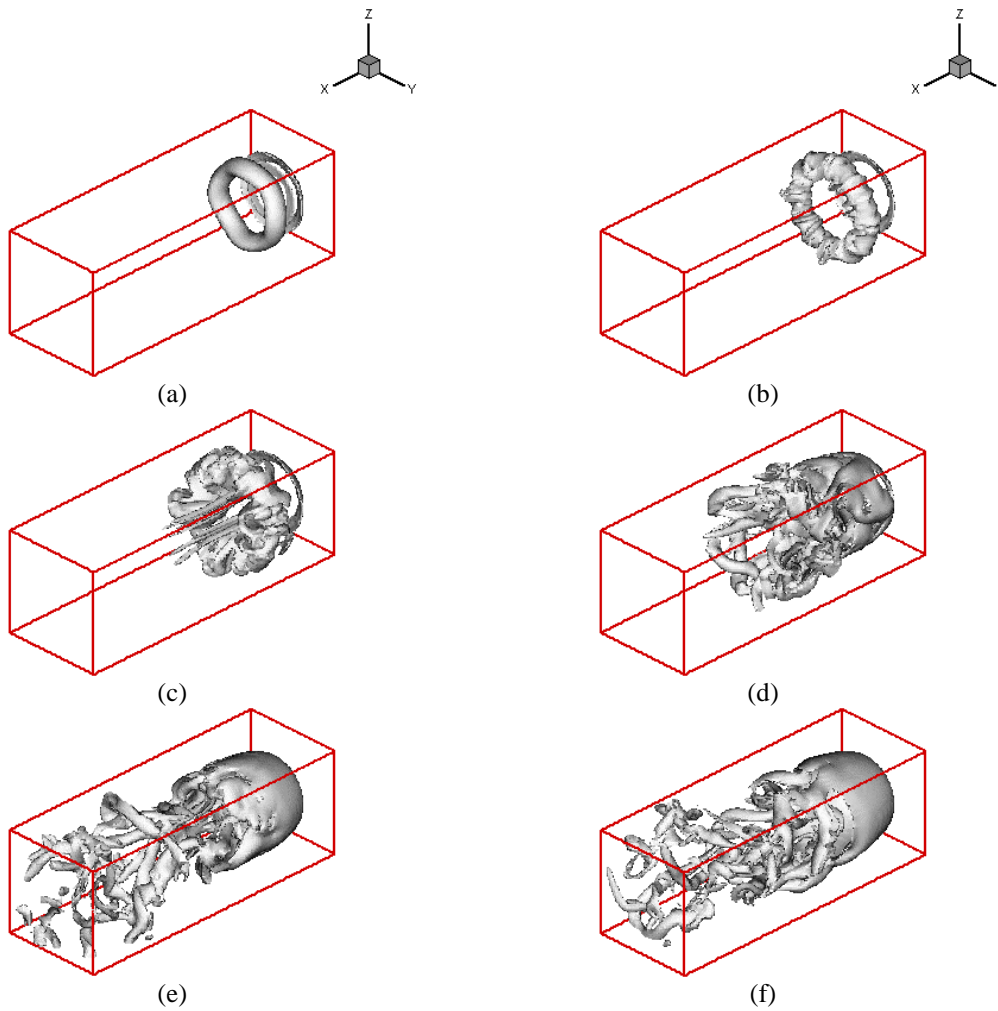
Figure 16. Vorticity Isosurfaces of Flow over Disk ($\mu = 0.15, \varepsilon = 0.3$)

(Isosurface Level = ± 0.25)
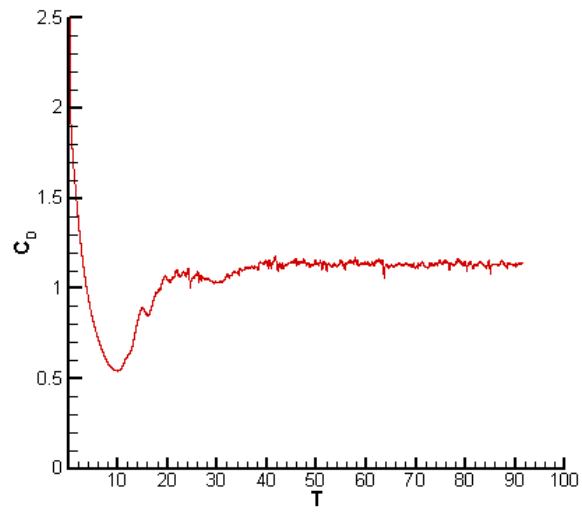
Figure 17. Coefficient of Drag History
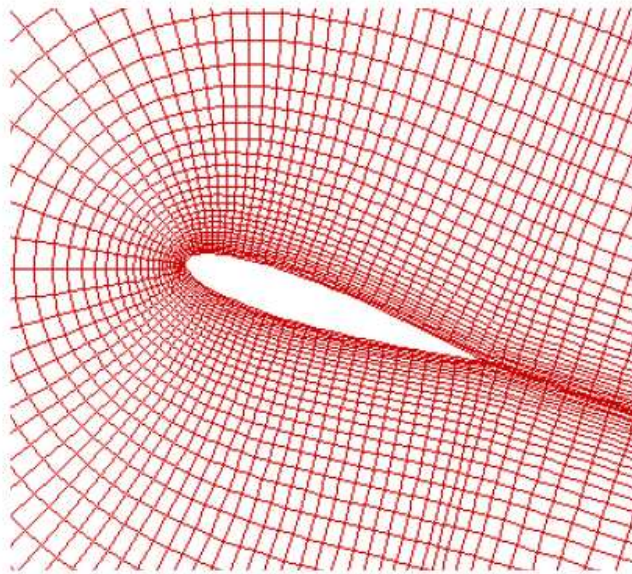
Figure 18. NACA 0015 Computational Grid
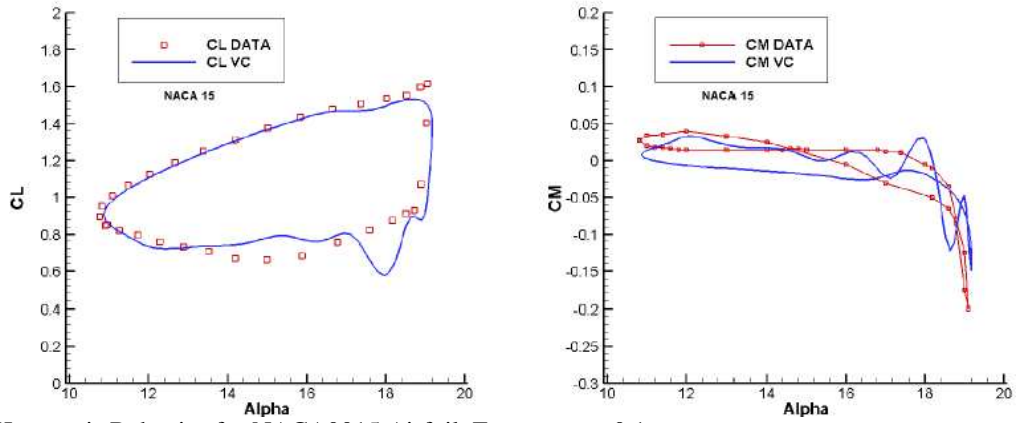
Figure 19. Hysteresis Behavior for NACA0015 Airfoil, Frequency = 0.1
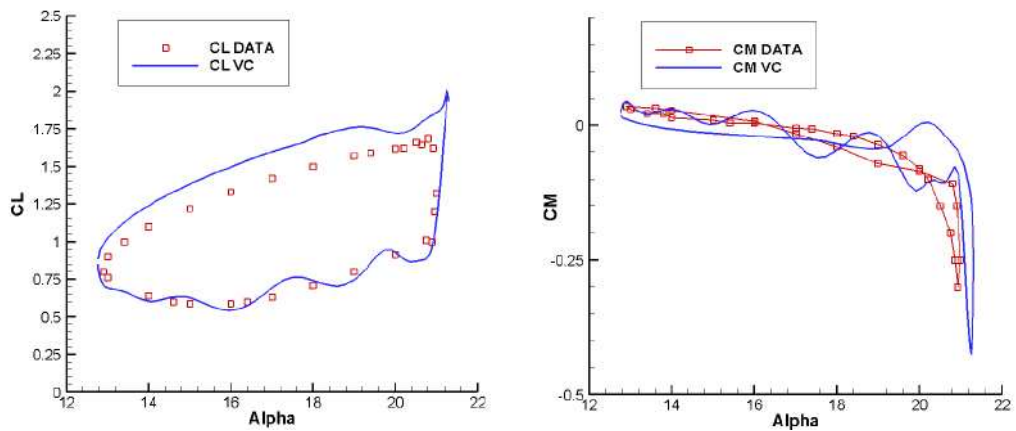
Figure 20. Hysteresis Behavior for NACA0015 Airfoil, Frequency = 0.13
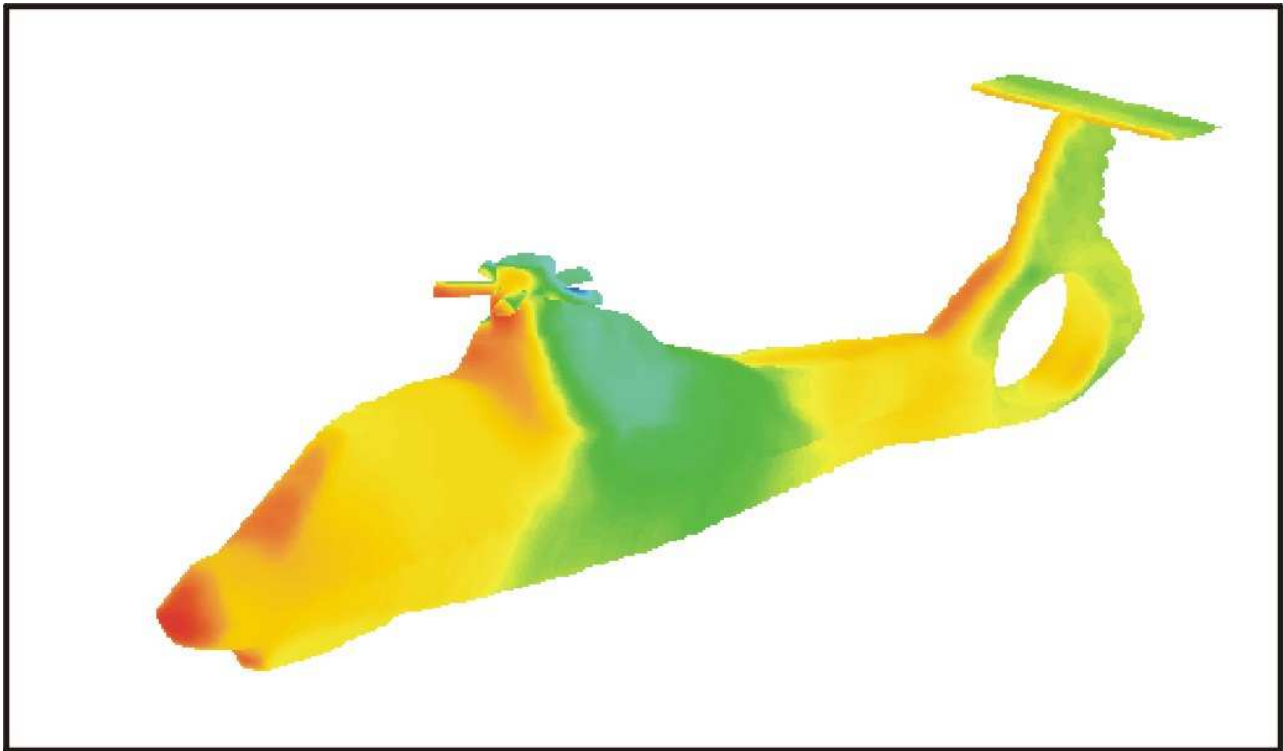
Figure 21. Interpolated surface pressure on the surface of the Comanche fuselage with rotating shanks
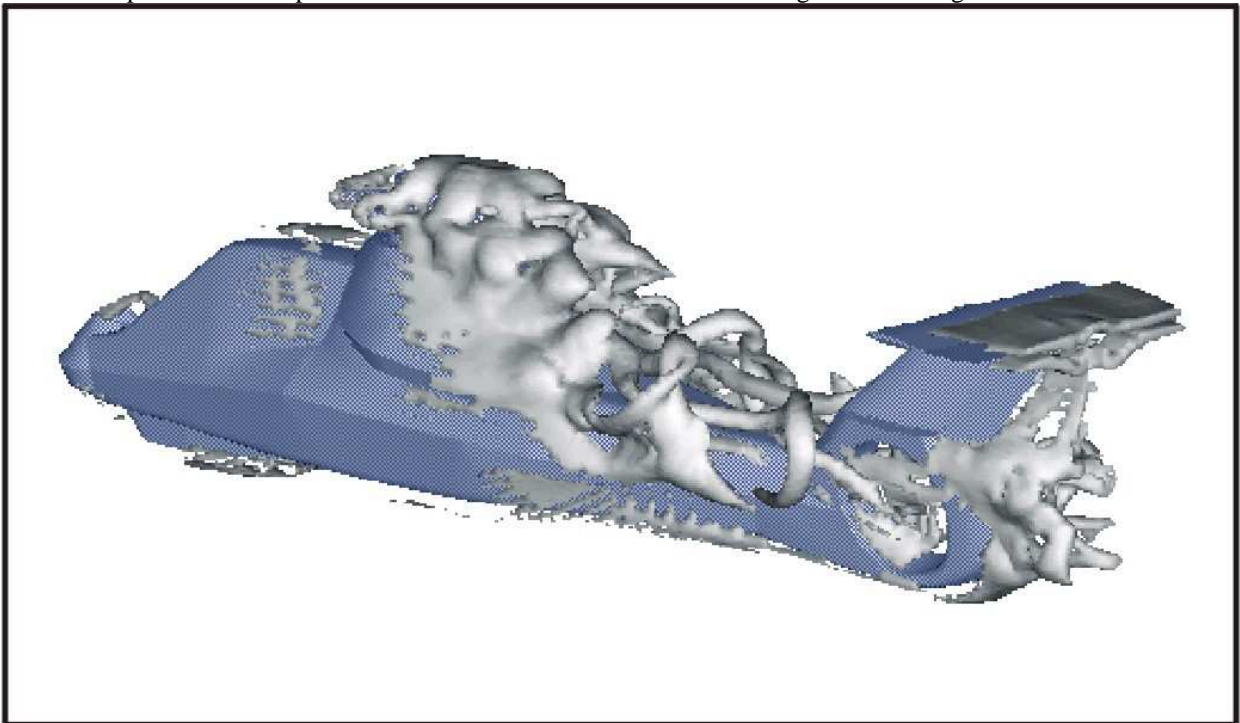
Figure 22. Computed Vorticity Isosurfaces for the Comanche Fuselage with Rotating Shanks
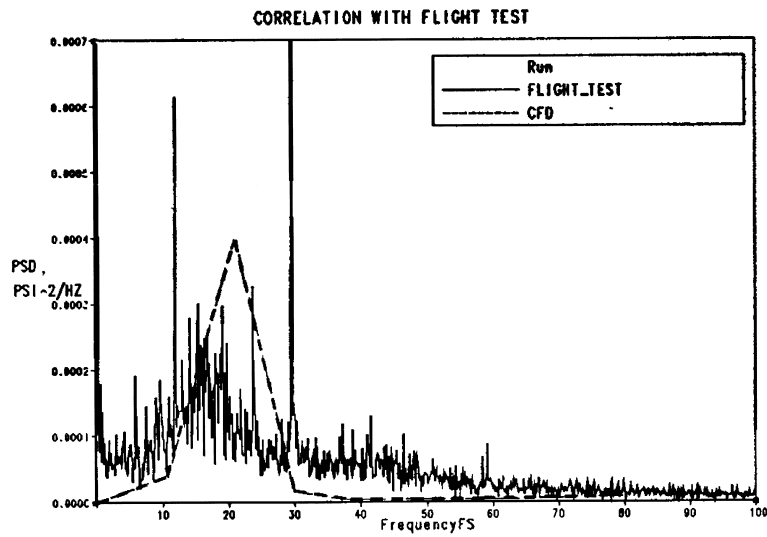
Figure 24. Comparison Between Computation and Flight Test of Power Spectrum of Pressure Fluctuations at Tail
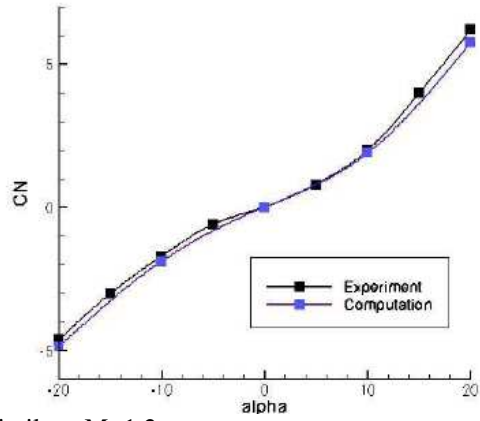
Figure 25. Pitching Moment for a Missile at M=1.2
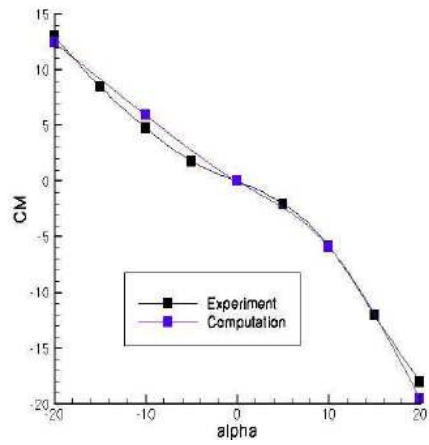
Figure 26. Pitching Moment for a Missile at M=1.2

a) Without Confinement

b) With Confinement

Figure 27. Isosurfaces of Vorticity Magnitude for a Missile Wake (M=1.2)